GLIA

WILEY

RESEARCH ARTICLE

Deletion of Alzheimer's disease-associated CD33 results in an inflammatory human microglia phenotype

Jannis Wißfeld[1] | Ichiro Nozaki[1,2] | Mona Mathews[1,3] | Tamara Raschka[4] |
Christian Ebeling[4] | Veit Hornung[5] | Oliver Brüstle[1,3] | Harald Neumann[1] ⓘ

[1]Institute of Reconstructive Neurobiology, University of Bonn Medical Faculty and University Hospital Bonn, Bonn, Germany

[2]Department of Neurology and Neurobiology of Aging, Kanazawa University Graduate School of Medical Sciences, Kanazawa, Japan

[3]LIFE & BRAIN GmbH, Cellomics Unit, Bonn, Germany

[4]Department of Bioinformatics, Fraunhofer Institute for Algorithms and Scientific Computing, Sankt Augustin, Germany

[5]Institute of Molecular Medicine, University of Bonn Medical Faculty and University Hospital Bonn, Bonn, Germany

Correspondence
Harald Neumann, Institute of Reconstructive Neurobiology, University of Bonn Medical Faculty and University Hospital Bonn, Venusberg-Campus 1, 53127 Bonn, Germany.
Email: harald.neumann@uni-bonn.de

Funding information
Deutsche Forschungsgemeinschaft, Grant/Award Number: FOR2953 no. 432190414; Innovative Medicines Initiative 2 Joint Undertaking, Grant/Award Number: PHAGO no. 115976

Abstract

Genome-wide association studies demonstrated that polymorphisms in the CD33/sialic acid-binding immunoglobulin-like lectin 3 gene are associated with late-onset Alzheimer's disease (AD). CD33 is expressed on myeloid immune cells and mediates inhibitory signaling through protein tyrosine phosphatases, but the exact function of CD33 in microglia is still unknown. Here, we analyzed *CD33* knockout human THP1 macrophages and human induced pluripotent stem cell-derived microglia for immunoreceptor tyrosine-based activation motif pathway activation, cytokine transcription, phagocytosis, and phagocytosis-associated oxidative burst. Transcriptome analysis of the macrophage lines showed that knockout of *CD33* as well as knockdown of the CD33 signaling-associated *protein tyrosine phosphatase, nonreceptor type 6* (*PTPN6*) led to constitutive activation of inflammation-related pathways. Moreover, deletion of *CD33* or expression of Exon 2-deleted CD33 (CD33$^{\Delta E2}$/CD33m) led to increased phosphorylation of the kinases spleen tyrosine kinase (SYK) and extracellular signal-regulated kinase 1 and 2 (ERK1 and 2). Transcript analysis by quantitative real-time polymerase chain reaction confirmed increased levels of *interleukin (IL) 1B*, *IL8*, and *IL10* after knockout of *CD33* in macrophages and microglia. In addition, upregulation of the gene transcripts of the AD-associated phosphatase *INPP5D* was observed after knockout of *CD33*. Functional analysis of macrophages and microglia showed that phagocytosis of aggregated amyloid-β_{1-42} and bacterial particles were increased after knockout of *CD33* or CD33$^{\Delta E2}$ expression and knockdown of *PTPN6*. Furthermore, the phagocytic oxidative burst during uptake of amyloid-β_{1-42} or bacterial particles was increased after *CD33* knockout but not in CD33$^{\Delta E2}$-expressing microglia. In summary, deletion of *CD33* or expression of CD33$^{\Delta E2}$ in human macrophages and microglia resulted in putative beneficial phagocytosis of amyloid β_{1-42}, but potentially detrimental oxidative burst and inflammation, which was absent in CD33$^{\Delta E2}$-expressing microglia.

KEYWORDS
Alzheimer's disease, CD33 (sialic-acid-binding immunoglobulin-like lectin 3 [SIGLEC3]), microglia, neuroinflammation, oxidative burst, phagocytosis, protein tyrosine phosphatase non-receptor type 6 (PTPN6)

Jannis Wißfeld and Ichiro Nozaki contributed equally to this study.

1 | BACKGROUND

Alzheimer's disease (AD) is a progressive neurodegenerative disease with amyloid burden (i.e., senile plaques), tau pathology (i.e., neurofibrillary tangles) and chronic innate immune dysfunction in the brain. Large-scale genome-wide association studies identified CD33 and other immune-related genes as risk factors for AD suggesting microglia to be key contributors to the disease (Bao, Wang, & Mao, 2016; Griciuc et al., 2013; Hollingworth et al., 2011; Malik et al., 2013). It was shown that amyloid β (Aβ) deposits contain sialic acid residues (Salminen & Kaarniranta, 2009; Szumanska, Vorbrodt, Mandybur, & Wisniewski, 1987), which could act as ligands for CD33/sialic acid-binding immunoglobulin-like lectin 3 (Alphey, Attrill, Crocker, & van Aalten, 2003; Freeman, Kelm, Barber, & Crocker, 1995; May, Robinson, Vinson, Crocker, & Jones, 1998). Furthermore, it was demonstrated that microglial CD33 expression levels positively correlate with the amount of Aβ and Aβ plaque load in the brains of AD patients (Griciuc et al., 2013). Moreover, humans with the polymorphic allele rs3865444(A) of CD33, which negatively correlates with AD, showed a reduction of both, surface expression of CD33 on microglia and Aβ deposition in their brains (Griciuc et al., 2013). It was reported that this CD33 variant rs3865444(A), which was associated with a slight decrease in risk for AD, is co-inherited with rs12459419(T), which modulates the splicing efficiency of Exon 2 in CD33 (Malik et al., 2013; Raj et al., 2014). Thereby, the IgV domain of CD33 that is encoded by Exon 2 and mediates sialic acid binding, is deleted. Thus, CD33 lacking Exon 2 (CD33$^{\Delta E2}$) cannot be activated by sialic acid ligands via the classical sialic acid binding site.

Like most of the CD33-related SIGLECs, CD33 mediates inhibitory signaling via the ITIM domains. Phosphorylation of the ITIM and ITIM-like domains of CD33 by Src family tyrosine kinases leads to recruitment and activation of phosphatases such as protein tyrosine phosphatase, nonreceptor type 6 and 11 (PTPN6 and 11, also known as Src homology region 2 domain-containing phosphatase 1 and 2, SHP1 and 2, respectively) or inositol polyphosphate-5-phosphatase D (INPP5D/SHIP1) (Avril, Floyd, Lopez, Vivier, & Crocker, 2004; Crocker & Redelinghuys, 2008; Lowell, 2011; Paul, Taylor, Stansbury, & McVicar, 2000; Taylor et al., 1999). These phosphatases are in theory able to modulate pro-inflammatory signaling originating from immunoreceptor tyrosine-based activation motifs (ITAMs). Inflammation, phagocytosis and radical production-inducing receptors such as triggering receptor expressed on myeloid cells 2 (TREM2), complement receptor 3 and signal regulatory protein β1 (SIRP-β1) interact upon activation with TYRO protein tyrosine kinase binding protein (TYROBP) (Gaikwad et al., 2009; Linnartz, Kopatz, Tenner, & Neumann, 2012; Takahashi, Rochford, & Neumann, 2005). TYROBP, which is also closely linked to AD (Zhang et al., 2013), contains an ITAM domain, which is phosphorylated by Src family tyrosine kinases upon interaction with ITAM-associated receptors. ITAM phosphorylation further results in recruitment of spleen tyrosine kinase (SYK) followed by activation of downstream signaling pathways including mitogen-activated protein kinases such as extracellular signal-regulated kinase 1 and 2 (ERK1 and 2) (Bourgin-Hierle, Gobert-Gosse, Therier, Grasset, & Mouchiroud, 2008; Lowell, 2011; Mocsai et al., 2006; Slack et al., 2007; Ziegenfuss et al., 2008). The activated downstream signaling via SYK can be attenuated by activation of SHP1 and SHP2 through ITIMs as counter-regulator (Crocker & Redelinghuys, 2008; Maeda et al., 1999; Maeda, Kurosaki, Ono, Takai, & Kurosaki, 1998). Several studies analyzed the role of CD33 in acute myeloid leukemia (reviewed in Walter, Appelbaum, Estey, & Bernstein, 2012); however, knowledge on the function of human CD33 in microglia, the only resident innate immune cell type of the brain, is still incomplete.

In the present study, we analyzed the transcriptional and functional alterations induced by loss of CD33 in human THP1 macrophages and CD33-deleted or CD33$^{\Delta E2}$-expressing human induced pluripotent stem cell-derived microglia (iPSdMiG). We demonstrate that deletion of CD33 and/or reduction of PTPN6/SHP1 triggers inflammatory gene transcription, phagocytosis and phagocytosis-associated oxidative burst in human macrophages and microglia.

2 | METHODS

2.1 | Human THP1 macrophage culture

THP1 cells have the characteristics of monocytes including cell surface markers and function, and can be differentiated into macrophage-like cells by stimulation with agents such as phorbol-12-myristate-13-acetate (PMA). THP1 cells were cultured in cell culture flasks with 5% CO_2 at 37°C. The medium for maintaining THP1 monocytes consisted of RPMI (Gibco), 100 μM penicillin/streptomycin (Gibco), 2 mM L-glutamine (Gibco), 1 mM sodium pyruvate (Gibco), 1% human N2-supplement (Gibco), and 1% heat-inactivated chicken serum (Gibco). Chicken serum was used since it does not contain N-glycolylneuraminic acid, which was found to be a xenobiotic for human cells (Raju et al., 2000; Varki, 2001). For differentiation of THP1 monocytes into adherent macrophages, the monocytes were incubated with 10 ng/ml PMA (Sigma-Aldrich) in cell culture plates for 48 hr, and then the attached THP1 cells were washed three times with medium to remove residual PMA. Subsequently, THP1 cells were cultured in medium without PMA for another 48 hr for further maturation toward macrophage phenotype.

2.2 | Generation of CD33 knockout (CD33$^{-/-}$) THP1 cells

The CD33$^{-/-}$ THP1 cells were generated by the clustered regularly interspaced short palindromic repeats (CRISPR)/CRISPR-associated protein-9 (Cas9) system. The targeting site of the single guide (sg) RNA with the sequence 5′-GACAACCAGGAGAAGATCGGGGG-3′ was in Exon 3 of CD33 obtained from an arrayed genome wide library (Schmidt, Schmid-Burgk, & Hornung, 2015), and knockout of CD33 was performed as previously reported (Schmidt, Schmid-Burgk,

Ebert, Gaidt, & Hornung, 2016). Briefly, THP1 cells were electroporated with two plasmids encoding the sgRNA and mCherry-Cas9, respectively. mCherry+ cells were enriched by cell sorting, and the sorted cells were plated under limiting dilution conditions to obtain single cell clones. The genotype was assessed by amplicon sequencing. For the analysis of the deep sequencing data, the genotyping software (www.OutKnocker.org) was utilized (Schmid-Burgk et al., 2014). The *CD33* knockout THP1 cell clone exhibited a four nucleotide deletion (GACAACCAGGAGAC−GGGGG) from position 566 to 569 in Exon 3 of *CD33* (Supplementary Figure S1a). The deletion of the CD33 protein was confirmed by flow cytometry.

2.3 | Generation of iPSdMiG

Human iPSdMiG were generated from induced pluripotent stem cells (iPSCs). The *CD33* knockout ($CD33^{-/-}$) and Exon 2-deleted CD33-expressing ($CD33^{\Delta E2}$) iPSC lines were generated isogenically from the wild-type (WT) BIONi010-C line (Rasmussen et al., 2014) under the nomenclature BIONi010-C-9 ($CD33^{-/-}$) and BIONi010-C-5 ($CD33^{\Delta E2}$; all lines were kindly provided by Janssen Pharmaceutica and deposited at EBiSC, European Bank for induced pluripotent Stem Cells, https://cells.ebisc.org). The cells were cultured in six-well plates coated with Geltrex (180 μg/ml in DMEM/F-12, Life Technologies) in TeSR-E8 medium (STEMCELL Technologies) and passaged with 0.5 mM EDTA in PBS (Sigma) or accutase (Gibco). To start the differentiation into iPSdMiG, iPSCs were cultured until 70–80% confluency and detached by 30 min collagenase IV treatment (1 mg/ml in DMEM/F-12, Gibco). Subsequently, they were transferred to noncoated culture dishes for embryoid body generation and differentiation into iPSdMiG. The differentiation protocol was carried out according to the established protocol at the LIFE & BRAIN GmbH (patent application number EP20162230). The iPSdMiG were produced from 4 to 6 weeks of differentiation and were harvested from the supernatant during the following 7-week peak production phase. Harvested iPSdMiG were plated onto poly-L-lysine-coated culture dishes and experiments were carried out 24 hr after plating.

2.4 | Lentiviral knockdown of *PTPN6*

Knockdown of *PTPTN6/SHP1* was achieved via viral transduction of THP1 cells with a pLKO.1 plasmid (TRCN0000006887, Open Biosystems) containing a short hairpin RNA (shRNA) against the target sequence (5′-CGACATGCTCATGGAGAACAT-3′). pLKO.1 empty vector was used as control vector (Open Biosystems). Production of viral particles was performed by transfection of HEK-293FT cells (Invitrogen) with packaging and *PTPN6* knockdown or empty vector control plasmids according to manufacturer's instructions. Briefly, 2.5×10^6 HEK-293FT cells were seeded onto poly-L-lysine (Sigma-Aldrich) precoated 100 mm cell culture dishes. Total of 50 μl Lipofectamine2000 (Invitrogen) and the plasmid mixture (5 μg pMD2G, 5 μg psPAX2 [Addgene] and 5 μg *PTPN6* knockdown or

control plasmid) were separately incubated in Opti-MEM (Gibco) for 5 min, then mixed together and incubated for 20 min at room temperature. Afterward, the preincubated transfection mix was added to the HEK-293FT cells and cultured in Opti-MEM + 10% fetal calf serum (FCS; Gibco) for 15 hr. Subsequently, the medium was changed to regular culture medium (DMEM containing 25 mM glucose (Gibco) supplemented with 100 μM nonessential amino acids (Gibco), 2 mM L-glutamine, 1 mM sodium pyruvate, and 10% FCS). The supernatant containing viral particles was collected 48 hr after transfection. WT and $CD33^{-/-}$ THP1 monocytes were incubated with the solution containing viral particles with either *PTPN6* knockdown (shPTPN6) or empty vector control (shCTRL) plasmids for 24 hr followed by a medium change and a 48 hr resting phase. Subsequently, treatment with 1 μg/ml puromycin for selecting transduced monocytes was performed. Puromycin selected cells were then differentiated into macrophages and the efficiency of *PTPN6* knockdown was examined by quantitative polymerase chain reaction (qPCR) and flow cytometry.

2.5 | Flow cytometry analysis

WT and $CD33^{-/-}$ THP1 monocytes with either shPTPN6 or shCTRL were seeded at a density of 3.0×10^6 in 10 cm dishes and differentiated as described above. For the analysis of surface marker expression, adherent monocyte-derived macrophages were mechanically detached and incubated with mouse anti-CD33 antibody (5 μg/ml, clone WM53, Abcam #ab30371) for 1 hr on ice. Isotype antibody mouse IgG1 (BD Pharmingen) was used as controls at corresponding concentration. Cell pellets were washed twice with PBS and incubated with phycoerythrin (PE)-conjugated goat anti-mouse IgG antibody (5 μg/ml, Jackson ImmunoResearch) for 30 min on ice. For intracellular staining of SHP1, the cells were fixed with 4% paraformaldehyde (PFA, Sigma-Aldrich) for 15 min at room temperature, and washed three times with PBS. Afterward, the cells were incubated with blocking solution containing 10% bovine serum albumin (BSA), 5% normal goat serum and 0.1% Triton-X100 (all Sigma-Aldrich) for 30 min at room temperature before adding the primary mouse anti-SHP1 antibody (2 μg/ml, clone D-11, Santa Cruz Biotechnology #SC-7289) or mouse IgG3 isotype control antibody (eBioscience). Analysis was performed with a FACS Calibur instrument (BD Biosciences) and FlowJo version 6.3.3 software (Tree Star). IPSdMiG were seeded at a density of $0.5-1 \times 10^6$ cells in six-well plates as described above. Then, 24 hr after seeding, the cells were mechanically detached using a cell lifter and incubated with FcR Blocking Reagent human (Miltenyi) in PBS for 15 min on ice. Afterward, rat anti-CD11B (5 μg/ml, clone M1/70, BD Pharmingen #550282), FITC-conjugated mouse anti-CD14 (1:20, clone HCD14, BioLegend #325604) mouse anti-CD33 antibody (5 μg/ml, clone HIM3-4, Exbio #11-365), APC-conjugated mouse anti-CD45 (1:20, clone HI30, BioLegend #304012), APC-conjugated mouse anti-FcγRI (1:50, clone 10.1, BioLegend #305013) or mouse anti-SIRP-α (5 μg/ml, clone SE7C2, Santa Cruz #sc-23863) were added to the cells into the FcR blocking mix and incubated for 1 hr on ice. Subsequently, the cells were washed twice with PBS and

incubated with Alexa647-conjugated goat anti-mouse IgG antibody (5 μg/ml, Jackson ImmunoResearch) or Alexa488-conjugated goat anti-rat (5 μg/ml, Invitrogen) for 30 min on ice. Measurements were performed on a BD Accuri C6 Plus and analyzed using FlowJo v10.

2.6 | RNA isolation

Prior RNA isolation, THP1 macrophages were treated with 1 μg/ml lipopolysaccaride (LPS; InvivoGen, *Escherichia coli* strain 0111:B4) for 24 hr or left untreated (UT). RNA was isolated from THP1 macrophages or iPSdMiG using the standard chloroform-phenol method. In short, the cells were incubated with QIAzol lysis reagent (Qiagen) and chloroform (Roth). After centrifugation, the upper colorless phase was transferred into new tubes containing equal volume of isopropanol (Roth). Finally, the RNA pellet was washed three times with 70% ethanol (Roth) and resolved in RNase-free DEPC water.

2.7 | RNA sequencing, differential expression, and pathway enrichment analysis

For RNA sequencing, total RNA was extracted using the RNeasy Mini Kit (Qiagen) according to manufacturer's instructions. The RNA concentration was measured and diluted to 100 ng/μl. RNA sequencing was performed in the NGS Core Facility of the University Hospital Bonn with 1×10^7 single-end reads per sample on a HiSeq 2500 V4 (Illumina). Reads were aligned to the *Homo sapiens* reference genome hg38 (GRCh38) with the ensemble gene annotation version 97 using STAR (v2.7.3a (Dobin et al., 2013)) with standard parameters and outFilterScoreMinOverLread 0.3 and outFilterMatchNminOverLread 0.3. Read count generation was performed using featureCounts/Subread (v2.0.0 (Liao, Smyth, & Shi, 2014)) ignoring multimapping reads. The differential gene expression analysis was performed with R (v3.5.2 (R Core Team, 2018)) in RStudio (v1.2.5042 (RStudio Team, 2015)) and the R package *DESeq2* (v1.22.2 (Love, Huber, & Anders, 2014)). As a first step, the data underwent a quality control, whereby transcripts with no counts were removed and outliers were detected. One sample from the group CD33$^{-/-}$ shPTPN6 was removed from further analysis due to very low overall counts. The differential gene expression analysis was performed afterward with the condition as contrast and log$_2$FC shrinkage using *apeglm* (v1.8.0 (Zhu, Ibrahim, & Love, 2019)). The top 100 differentially expressed genes are shown in Supplementary Table S2. Across these conditions, four pairwise comparisons were done (1. WT shCTRL v CD33$^{-/-}$ shCTRL, 2. WT shPTPN6 v CD33$^{-/-}$ shPTPN6, 3. WT shCTRL v WT shPTPN6, 4. CD33$^{-/-}$ shCTRL v CD33$^{-/-}$ shPTPN6). After the differential expression analysis, the Ensembl IDs were mapped to HGNC identifiers via the R package *org.Hs.eg.db* (v3.8.2, (Carlson, 2019)). Plots were created using *ggplot2* (v3.2.1 (Wickham, 2016)). KEGG pathway enrichment analyses were performed using *clusterProfiler* (v3.14.0 (Yu, Wang, Han, & He, 2012)) with log$_2$FC ≥ 1 and FDR-adjusted *p*-value ≤.01.

2.8 | qPCR analysis

Isolated RNA was reverse transcribed to cDNA using superscript III reverse transcriptase (Invitrogen) following manufacturer's instructions. In short, RNA was incubated with random hexamer primers (Roche) and deoxynucleotide mixture (Peqlab) at 65°C for 5 min. Afterward, single strand buffer (Invitrogen), dithiothreitol (Invitrogen) and superscript III reverse transcriptase (Invitrogen) were added. The conversion of RNA to cDNA was performed with a T3 Thermocycler (Biometra). The gene transcription levels of *CD33*, interleukin (IL) 1β/*IL1B*, *IL6*, *IL8*, *IL10*, SHIP1/*INPP5D*, SHP1/*PTPN6*, SHP2/*PTPN11*, SIRP-α/*SIRPA*, tumor necrosis factor α (TNF-α)/*TNFA*, and *TYROBP* were analyzed by qPCR. *Glyceraldehyde 3-phosphate dehydrogenase* (*GAPDH*) was used as house-keeping gene. SYBR Green PCR Master Mix (Applied Biosystems) was used in addition to 200 ng of cDNA and the respective gene-specific primers (Supplementary Table S1). For *IL10* and *TNFA* the primer sequences were used from previous published papers (Brosig et al., 2015; Krakauer, Sorensen, Khademi, Olsson, & Sellebjerg, 2008). Using an ABI 5700 Sequence Detection System (PerkinElmer) the amplification was performed as follows: 95°C, 10 s; 40 cycles of 95°C for 15 s, 60°C for 30 s, and 72°C for 30 s. Relative gene transcription was quantified using the ΔΔCT method with *GAPDH* as internal control. Each value was normalized to the WT control condition.

2.9 | Detection of phosphorylated SYK and ERK1/2 in THP1 macrophages

Quantification of phosphorylated SYK and ERK1/2 in THP1 macrophages was performed via Western blot analysis. Therefore, 8.0×10^6 cells of WT and CD33$^{-/-}$ THP1 monocytes were seeded in 150 mm culture dishes and differentiated as described above. The differentiated THP1 macrophages were treated with either 10 μg/ml anti-FcγRI (CD64) antibody (clone 10.1, Santa Cruz Biotechnology #SC-1184), 10 μg/ml anti-FcγRI antibody combined with 10 μg/ml mouse IgG1 isotype control or combined with 10 μg/ml mouse anti-CD33 antibody (clone 1C7/1, Cedarlane #CL7627AP) for 5 min (SYK detection) or 10 min (ERK1/2 detection) at 37°C. CD33 antibody clone 1C7/1 was previously described as putative agonistic antibody (Taylor et al., 1999). Furthermore, we tested whether this antibody stimulates CD33 by using a reporter cell line system (Supplemental Methods and Supplementary Figure S2). The cells were mechanically detached and dissolved using radio immunoprecipitation assay buffer (Sigma-Aldrich) containing 2% Halt phosphatase inhibitor cocktail (Thermo Scientific) for 1 hr on ice followed by centrifugation to remove cellular debris. Dynabeads (Invitrogen) were prepared according to the manufacture's protocol. Briefly, protein A-conjugated Dynabeads were incubated with rabbit anti-total SYK (tSYK) antibody (1:250, Cell Signaling Technology #2712) or anti-total ERK1/2 (tERK1/2) antibody (1:100, Cell Signaling Technology #4695) for 2 hr at 4°C. The supernatant of the cell lysate was incubated with the antibody-Dynabeads complex for 1 hr at 4°C. The samples were heat denatured at 70°C for 10 min after washing and suspending with elution buffer. The samples were loaded with NuPAGE

LDS Sample Buffer (Invitrogen) on a NuPAGE 10% Bis-Tris polyacryl-amide gel (Invitrogen) and SDS-PAGE was performed in NuPAGE MES SDS Running Buffer using the XCell *SureLock* Mini-Cell (Invitrogen, 90 min run time at 130 V constantly on ice). Afterward, Western Blot was performed using a nitrocellulose membrane with pore size of 0.45 μm (Bio-Rad) in NuPAGE transfer buffer containing 10% methanol using XCell II Blot Module (Invitrogen, 1 hr run time at 380 mA constantly on ice). The blotted membrane was blocked in Tris buffered saline containing 0.05% Tween-20 (TBS-T) for 1 hr at room temperature, and then incubated with rabbit anti-phospho-SYK (pSYK) antibody (1:500, clone 87C1, Tyr525-526, Cell Signaling Technology #2710) or rabbit anti-phospho-pERK1/2 (pERK1/2) antibody (1:1000, clone 20G11, Thr202/Tyr204, Cell Signaling Technology #4376), overnight at 4°C. Then, the membrane was incubated with goat-anti-rabbit IgG horseradish peroxidase (HSP)-conjugated antibody (1:10,000; Jackson ImmunoResearch) for 1 h at room temperature. The bands on the membrane were detected by the *ChemiDoc XRS+ system with Image Lab software* (Bio-Rad) using SuperSignal West Pico Chemiluminescent substrate (Pierce). After stripping with Restore PLUS Western Blot Stripping buffer (Thermo Scientific), the membrane was incubated with the corresponding anti-tSYK (Cell Signaling Technology) or anti-tERK1/2 antibody (Cell Signaling Technology) overnight at 4°C followed by secondary antibody staining with goat-anti-rabbit IgG HSP. The density of each band was analyzed by Image Lab 4.0.1 software (Bio-Rad). The ratios of pSYK to tSYK and pERK1/2 to tERK1/2 were calculated in each experimental group and normalized to the ratio of WT UT condition.

2.10 | Detection of phosphorylated SYK in iPSdMiG

In total, 2×10^4 iPSdMiG were plated per well in poly-L-lysine-coated 96 well plates (Corning) as described above. Then, 24 hr after plating, the cells were stimulated for 5 min with anti-TREM2 (5 μg/ml, R&D Systems #AF1828), corresponding IgG isotype control (5 μg/ml Abcam #ab224187) or left untreated. pSYK levels were detected by the AlphaLISA SureFire Ultra p-SYK (Tyr525/526) Assay Kit (PerkinElmer) and normalized to the values of tSYK using the AlphaLISA SureFire Ultra Total SYK Assay Kit (PerkinElmer) according to the two-plate assay protocol for adherent cells. All samples were measured as technical duplicates in 384-well OptiPlates (PerkinElmer). The plate was measured using the standard AlphaLISA settings on a PerkinElmer EnVision 2104 system. For the analysis, the technical duplicates were averaged and the pSYK signal was normalized to the tSYK signal. The Data was displayed as pSYK/tSYK relative to the WT signal.

2.11 | Phagocytosis of aggregated Aβ$_{1-42}$ and cellular debris

Prior to phagocytosis and reactive oxygen species (ROS) experiments, aggregated Aβ$_{1-42}$ and cellular debris were prepared. Aβ$_{1-42}$ or biotinylated Aβ$_{1-42}$ (Bachem) were incubated for 72 hr at 37°C to cause

formation of aggregated structures. For the generation of cellular debris, ARPE-19 cells (ATCC) were treated by 40 nM okadaic acid (Sigma-Aldrich) for 24 hr. The cellular debris was treated by DNase and for phagocytosis, it was additionally stained with DiI-Derivatives for Long-Term Cellular Labeling (Invitrogen) according to the manufacturer's instructions. Phagocytosis experiments were performed as previously reported (Shahraz et al., 2015). Briefly, 7×10^4 THP1 monocytes were seeded per chamber of a four-chamber culture slide and differentiated as described above. IPSdMiG were seeded at a density of 2×10^4 cells per well of a 96-well μ-plate (ibidi). The cells were incubated with 2 μM aggregated biotinylated Aβ$_{1-42}$ or 5 μg/ml DiI-labeled cellular debris for 90 min. Afterward, the cells were washed and fixed with 4% PFA for 15 min, followed by incubation with blocking solution containing 10% BSA, 5% normal goat serum and 0.1% Triton-X100 (all Sigma-Aldrich) for 1 hr at room temperature. Then, THP1 macrophages were incubated with rat anti-CD11b (2.5 μg/ml, BD Pharmingen #553308) and iPSdMiG with rabbit anti-IBA1 (2 μg/ml, Synaptic Systems #234003) overnight at 4°C and subsequently with Alexa 488-conjugated anti-rat or anti-rabbit IgG (2.5 μg/ml, Invitrogen) and Cy3-conjugated streptavidin (2.5 μg/ml, Jackson ImmunoResearch, only for biotinylated Aβ$_{1-42}$) for 2 hr at room temperature. For each condition, five images were randomly taken using confocal laser scanning microscopy (Fluoview 1000, Olympus). The images were analyzed using ImageJ version 1.49 (NIH) to calculate the ratio of Aβ$_{1-42}$- or cellular debris-positive cells to the total number of cells. Each ratio was normalized to the WT control.

2.12 | Phagocytosis of bacterial particles

THP1 macrophages were seeded at a density of 7×10^4 cells per chamber of a four-chamber culture slide and incubated with 1 mg/ml pHrodo Red *Staphylococcus aureus* BioParticles conjugates (Thermo Fisher #A10010) for 120 min at 37°C according to manufacturer's instructions. After washing the cells, they were fixed with 4% PFA containing 0.25% glutaraldehyde for 15 min and mounted on cover slips. Five pictures were randomly taken for each experimental condition by confocal laser scanning microscopy. IPSdMiG were seeded at a density of 2×10^4 cells per well of a 96-well μ-plate (ibidi) as described above. Subsequently, iPSdMiG were incubated with 0.5 mg/ml pHrodo Red *S. aureus* BioParticles conjugates for 90 min at 37°C according to manufacturer's instructions. Afterward, the cells were incubated with Hoechst 33342 (5 μg/ml, Invitrogen) for 10 min at 37°C and analyzed by live cell imaging using an IN Cell Analyzer 2200 system. The intensity from the collected images was measured by Image J version 1.49. The background intensity was subtracted from the image intensity and then normalized to the WT condition.

2.13 | Detection of the phagocytosis-associated oxidative burst

Analysis of the oxidative burst was performed as previously described (Shahraz et al., 2015). In short, THP1 cells were seeded at

a density of 7×10^4 cells per chamber of a four-chamber culture slide and iPSdMiG at a density of 2×10^4 cells per well of a 96-well μ-plate (ibidi). Then, 24 hr prior to the experiment, the medium of the THP1 macrophages was changed to serum-free medium. As controls the differentiated THP1 cells were preincubated with either 20 μg/ml superoxide dismutase 1 (SOD1; Serva) or 40 μM Trolox (Cayman) for 1 hr at 37°C. Subsequently, the cells were treated with 10 μM aggregated $A\beta_{1-42}$ or 5 μg/μl cellular debris for 15 min at 37°C. iPSdMiG were preincubated with 4 mM N-acetyl-L-cysteine (NAC, Sigma) for 1 h at 37°C followed by treatment with 200 μg/ml nonlabeled *S. aureus* BioParticles (Thermo Fisher) with or without the scavenger NAC for 15 min at 37°C. After removing the supernatant, all conditions were treated with 30 μM dihydroethidium (DHE, Invitrogen) in Krebs-HEPES-buffer for 15 min at 37°C. Then, the cells were fixed with 4% PFA containing 0.25% glutaraldehyde (Sigma-Aldrich) for 15 min at room temperature. At least five images were randomly taken for each condition by confocal laser scanning microscopy or using an IN Cell Analyzer 2200 system, and DHE intensity from the collected images was evaluated by Image J version 1.49. The background intensity was subtracted and the DHE intensity in each experimental condition was normalized to the WT condition.

2.14 | Statistical analysis

Data are shown as mean value + *SEM*. Data were examined for normal distribution by Shapiro–Wilk test and for equality of variances by Levene's test prior to analysis. Differences were analyzed using one-way or two-way analysis of variance (ANOVA) combined with Bonferroni post hoc test and Welch ANOVA followed by Games–Howell post hoc test if equality of variances could not be guaranteed as indicated. * represents $p \leq .05$, ** represents $p \leq .01$ and *** represents $p \leq .001$. Statistical analysis was performed using Stata version 15 (Stata Corp.) or SPSS version 23 (IBM).

3 | RESULTS

3.1 | Deletion of *CD33* and knockdown of *PTPN6* in THP1 macrophages

CD33 knockout ($CD33^{-/-}$) THP1 macrophages were generated by the CRISPR/Cas9 technique by deleting four base pairs in Exon 3 (Supplementary Figure S1a). *CD33* knockout THP1 macrophages showed loss of extracellular CD33 expression compared to WT shCTRL, as demonstrated by flow cytometry analysis (Figure 1a,b and S1b; WT shCTRL 100 ± 23.1%, WT shPTPN6 129.8 ± 24.3%, $CD33^{-/-}$ shCTRL 6.1 ± 1.5% with $p = .031$ and $CD33^{-/-}$ shPTPN6 3.5 ± 1.4% with $p = .026$). Similarly, *CD33* gene transcripts were diminished in $CD33^{-/-}$ THP1 macrophages (Figure 1c; WT shCTRL 1.00 ± 0.02, WT shPTPN6 1.33 ± 0.24, $CD33^{-/-}$ shCTRL 0.02 ± 0.01 with $p < .001$

and $CD33^{-/-}$ shPTPN6 0.03 ± 0.01 with $p < .001$). Likewise, shRNA-mediated knockdown of *PTPN6* (*SHP1*) was examined. Expression and transcription levels of *PTPN6* were strongly decreased in WT and $CD33^{-/-}$ macrophages after knockdown with short hairpin lentiviral vectors for *PTPN6* (shPTPN6) compared to WT and $CD33^{-/-}$ macrophages transduced with an empty vector control (shCTRL) (Figure 1d–f; protein level: WT shCTRL 100 ± 21.16%, WT shPTPN6 37.45 ± 13.16%, $CD33^{-/-}$ shCTRL 104.76 ± 5.27% and $CD33^{-/-}$ shPTPN6 51.19 ± 11.64%; gene transcription level: WT shCTRL 1.00 ± 0.01, WT shPTPN6 0.05 ± 0.03 with $p < .001$, $CD33^{-/-}$ shCTRL 1.11 ± 0.16 and $CD33^{-/-}$ shPTPN6 0.10 ± 0.01 with $p < .001$).

Thus, THP1 macrophages with *CD33* deletion and an additional knockdown of the downstream molecule *PTPN6* were successfully validated to study function of CD33. Further, CD33 tended to be upregulated upon *PTPN6* knockdown without statistical significance.

3.2 | Increased inflammatory transcriptome profile after *CD33* knockout or *PTPN6* knockdown

RNA sequencing was performed on samples obtained from cultured THP1 macrophages (WT shCTRL, WT shPTPN6, $CD33^{-/-}$ shCTRL, and $CD33^{-/-}$ shPTPN6) to investigate how *CD33* knockout and/or *PTPN6* knockdown affect the transcriptome profile. Principal component analysis showed clustering of the four individual groups, representing the genotypes WT and $CD33^{-/-}$, as well as the treatments shCTRL and shPTPN6. Knockout of *CD33* led to stronger transcriptome profile changes than the knockdown of *PTPN6*, as shown by the higher variance of PC1 compared to PC2 (Figure 2a; PC1 71.5% and PC2 23.7%). Knockout of *CD33* (WT shCTRL vs. $CD33^{-/-}$ shCTRL) affected expression of 2,724 genes ($|\log_2 FC| \geq 1$, padj ≤ 0.05), which was comparable to the knockdown of *PTPN6* in WT macrophages (2,342 differentially expression [DE] genes). However, knockdown of *PTPN6* in *CD33*-deficient background ($CD33^{-/-}$ shCTRL vs. $CD33^{-/-}$ shPTPN6) resulted in only 1,042 DE genes indicating a less considerable effect of *PTPN6* knockdown in $CD33^{-/-}$ macrophages. Further, comparison of the expression profile of the top 200 most varying genes and applying hierarchical clustering to groups and genes also indicated a higher similarity of $CD33^{-/-}$ shCTRL and $CD33^{-/-}$ shPTPN6 and a substantial difference between the WT and $CD33^{-/-}$ samples (Figure 2b). Pathway enrichment analysis using upregulated genes ($\log_2 FC \geq 1$ and FDR-adjusted p-value $\leq .01$) and the KEGG database predominantly identified upregulated inflammation-related pathways, such as "TNF signaling pathway," "IL-17 signaling pathway," and "NF-kappa B signaling pathway" if *CD33* was knocked out (Figure 2c; comparison 1: WT shCTRL vs. $CD33^{-/-}$ shCTRL and comparison 2: WT shPTPN6 vs. $CD33^{-/-}$ shPTPN6). Further, *PTPN6* knockdown in WT macrophages (comparison 3: WT shCTRL vs. WT shPTPN6) also showed
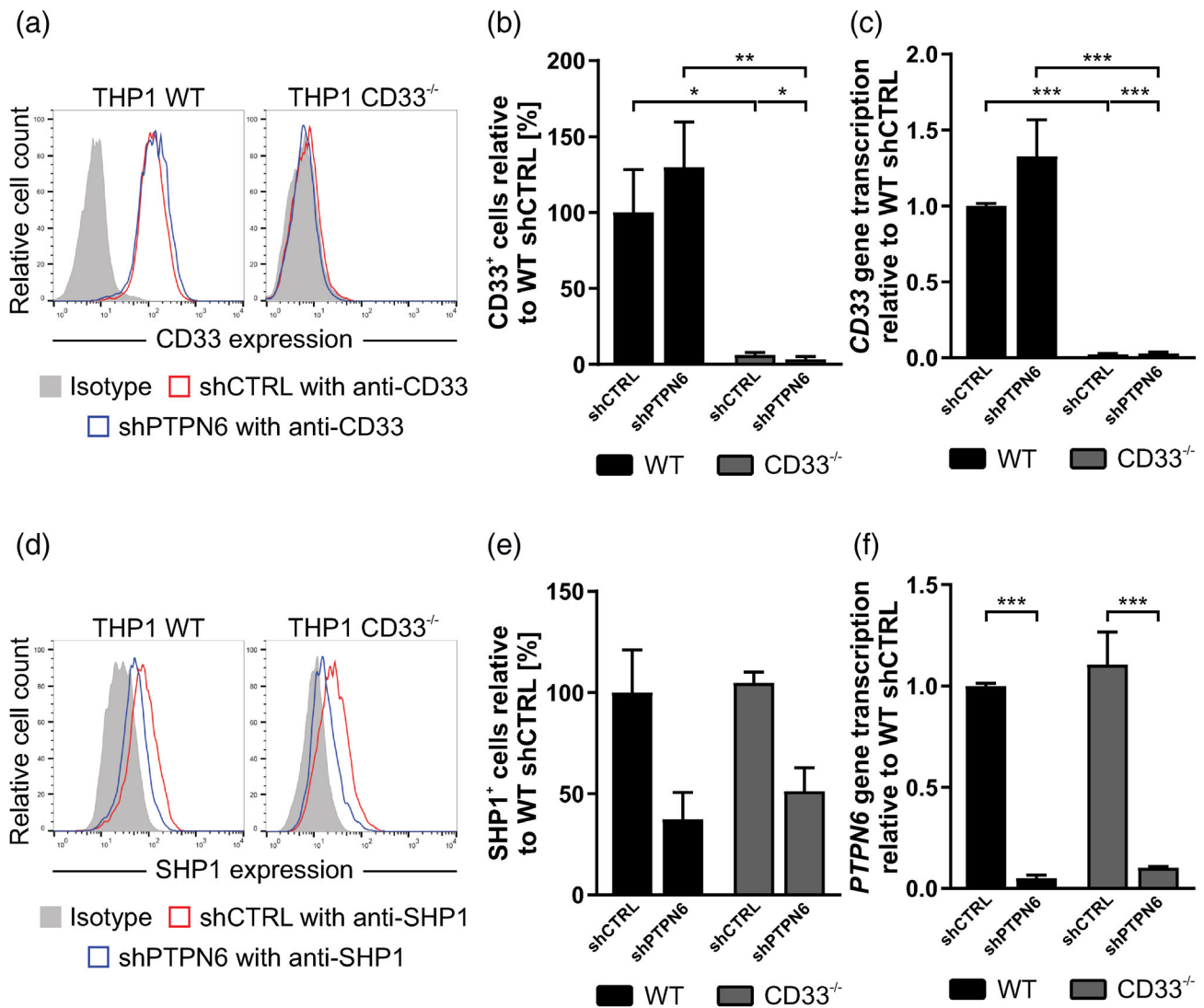
FIGURE 1 *CD33* knockout (CD33$^{-/-}$) and lentiviral shRNA-mediated *PTPN6* knockdown in THP1 macrophages. (a) Exemplary flow cytometry histogram graph showing expression levels of CD33 in wild type (WT) and CD33$^{-/-}$ macrophages. CD33 expression is absent in CD33$^{-/-}$ macrophages. These graphs were the representative data out of five independent experiments. (b) Quantification of CD33 expression in THP1 macrophages. CD33 surface expression levels were nearly diminished in CD33$^{-/-}$ macrophages (dark gray) regardless of knockdown of *PTPN6* (shPTPN6). Data are shown as mean + *SEM* ($n = 5$). **$p \leq .01$, *$p \leq .05$ determined by two-way analysis of variance (ANOVA) followed by Bonferroni post hoc test. (c) *CD33* gene transcripts analyzed by semiquantitative real-time polymerase chain reaction (PCR) in human THP1 macrophages. *CD33* levels were diminished in both, shCTRL and shPTPN6 CD33$^{-/-}$ THP1 macrophages (dark gray). Data are shown as mean + *SEM* ($n = 4$). ***$p \leq .001$ determined by two-way ANOVA followed by Bonferroni post hoc test. (d) SHP1 protein levels were assessed via flow cytometry in WT and CD33$^{-/-}$ macrophages with knockdown of *PTPN6*. Short hairpin *PTPN6* knockdown lentiviral vector transfected cells (shPTPN6) exhibited diminished SHP1$^+$ cells (blue line) compared to the control vector transfected cells (red line) in both, WT (left) and CD33$^{-/-}$ (right) THP1 macrophages. Representative image of three independent experiments. (e) Quantification of SHP1 expression in THP1 macrophages. SHP1 expression levels were decreased in short hairpin *PTPN6* knockdown lentiviral vector transfected cells (shPTPN6) compared to the control vector transfected cells (shCTRL) in both, WT (black) and CD33$^{-/-}$ (dark gray) THP1 macrophages. Data are shown as mean + *SEM* ($n = 3$). (f) Gene transcription levels of *PTPN6* were analyzed by semiquantitative real-time PCR in WT and CD33$^{-/-}$ THP1 macrophages. *PTPN6* mRNA levels were decreased following knockdown of *PTPN6* (shPTPN6), in both, WT (black) and CD33$^{-/-}$ (dark gray) THP1 macrophages. Data are shown as mean + *SEM* ($n = 4$). ***$p \leq .001$ determined by two-way ANOVA followed by Bonferroni post hoc test

an overall inflammation-related scenario sharing the majority of upregulated pathways with the WT versus CD33$^{-/-}$ comparisons. Interestingly, when analyzing *PTPN6* knockdown in a CD33$^{-/-}$ background (comparison 4: CD33$^{-/-}$ shCTRL vs. CD33$^{-/-}$ shPTPN6), no pathways were significantly upregulated in this comparison, and thus clearly differed from the three previous comparisons (Figure 2c).

Taken together, knockout of *CD33* as well as knockdown of *PTPN6* in a WT but not *CD33*-deficient background led to upregulation of inflammation-related pathways.
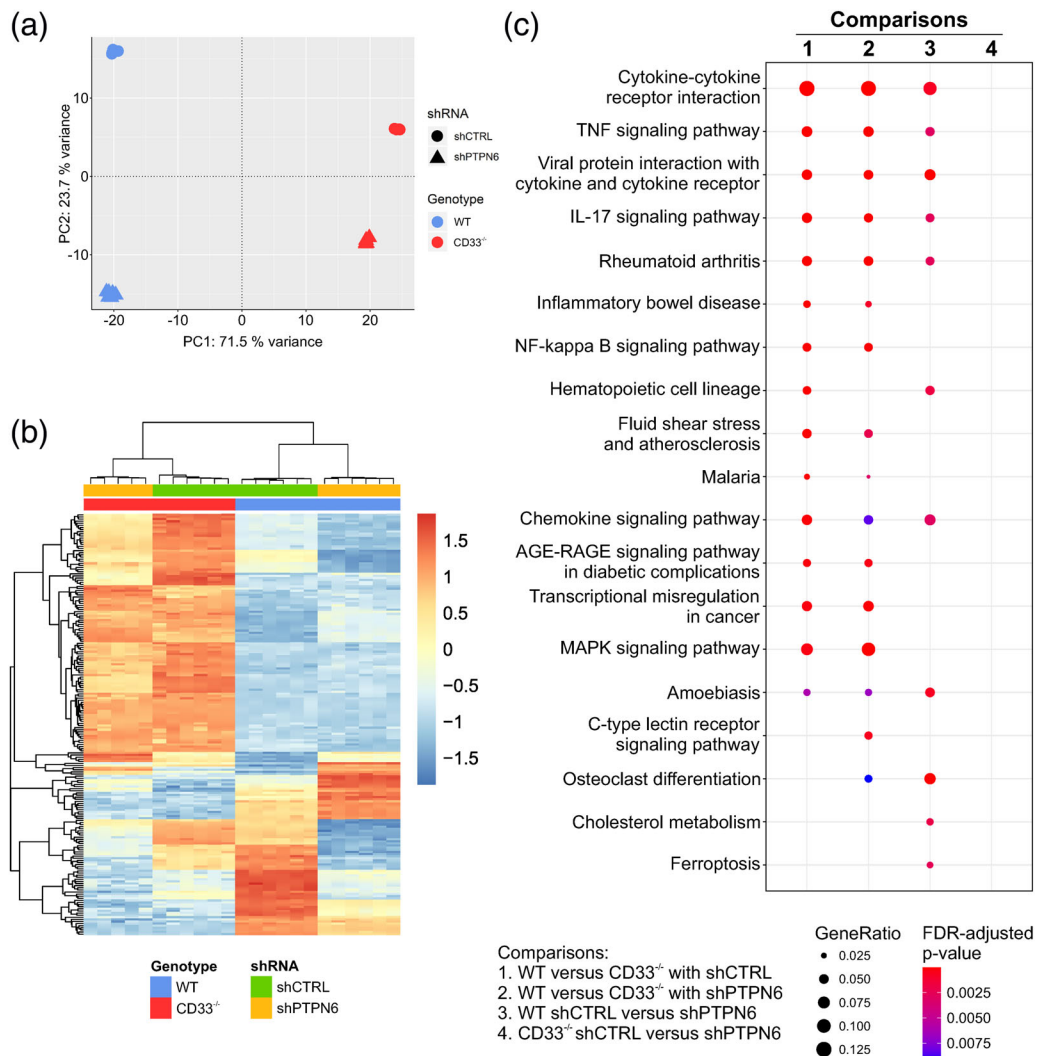
FIGURE 2 Transcriptome analysis of *CD33* knockout and *PTPN6* knockdown in THP1 macrophages. (a) Principal component analysis (PCA) of THP1 macrophage RNA sequencing. PCA resulted in four clusters representing the four individual groups wild type (WT) shCTRL, WT shPTPN6, CD33$^{-/-}$ shCTRL CD33$^{-/-}$ shPTPN6. (b) Heatmap of the top 200 most varying genes with hierarchical clustering for rows and columns stressed that the most extreme differences were between WT and CD33$^{-/-}$. Minor changes were observed for *PTPN6* knockdown. (c) Dotblot of KEGG pathway enrichment analysis revealed an upregulation of the inflammation-related transcription profile in comparisons 1–3 (i.e., 1. WT shCTRL vs. CD33$^{-/-}$ shCTRL, 2. WT shPTPN6 vs. CD33$^{-/-}$ shPTPN6, 3. WT shCTRL vs. WT shPTPN6) but not in comparison 4 (CD33$^{-/-}$ shCTRL vs. CD33$^{-/-}$ shPTPN6)

3.3 | Activated SYK and ERK1/2 signaling pathways in *CD33*-deficient THP1 macrophages and iPSdMiG

Loss of inhibitory CD33 signaling through knockout of *CD33* might change the activation pattern of the ITAM signaling pathway and thus might induce inflammation. Our transcriptome profile analysis of THP1 macrophages suggested that CD33 influences several inflammatory pathways (Figure 2c). Thus, we studied the activation of SYK and ERK1/2, two ITAM signaling-associated kinases, by assessing their phosphorylation status. Further, we co-stimulated THP1 macrophages with cross-linking antibodies for the ITAM-associated receptor FcγRI and for CD33. The CD33 antibody clone 1C7/1 was first confirmed to activate CD33 using a CD33 reporter cell line, in which the

extracellular part of CD33 was fused to the activatory molecule DAP12/TYROBP. Thus, in this cellular system CD33 activation should result in an increase in intracellular calcium levels. Indeed, the CD33 reporter cell line exhibited increased intracellular calcium levels upon treatment with CD33 antibody clone 1C7/1 as demonstrated by the antibody-triggered increase in fluorescence intensity of the calcium-sensitive dye Rhod-3 (Supplemental Figure S2).

Western Blot analysis of THP1 cell lysates revealed that phosphorylated ERK1/2 was increased in UT CD33$^{-/-}$ macrophages compared to UT WT macrophages (Figure 3a,b; WT UT 1.00 ± 0.10 compared to CD33$^{-/-}$ UT 1.58 ± 0.09 with $p = .043$). Next, we tested whether activation of inhibitory CD33 signaling by the antibody clone 1C7/1 could counteract cellular activation induced by activation of FcγRI. Cross-linking of FcγRI slightly increased ERK1/2

phosphorylation in WT THP1 macrophages (Figure 3a,b; anti-FcγRI 1.46 ± 0.10) and co-stimulation of CD33 appeared to interfere with this stimulation (anti-FcγRI + isotype antibody 1.38 ± 0.08 compared to anti-FcγRI + anti-CD33 1.17 ± 0.08), although both effects were not significant.

Similar to ERK1/2, the CD33$^{-/-}$ THP1 macrophages exhibited an increase in phosphorylated SYK to total SYK ratio compared to UT WT THP1 macrophages (WT UT 1.00 ± 0.03 compared to CD33$^{-/-}$ UT 2.57 ± 0.35 with p = .019). Again, pSYK also showed a slight but not significant increase after activation of FcγRI in WT THP1 macrophages (Figure 3c,d; anti-FcγRI 1.91 ± 0.05), which in turn also exhibited slightly but not significant decreased pSYK levels upon simultaneous treatment with anti-CD33 antibody (anti-FcγRI + isotype antibody 1.86 ± 0.29 compared to anti-FcγRI + anti-CD33 1.49 ± 0.27). Cross-linking of FcγRI did not have any effect on SYK or ERK1/2 phosphorylation in CD33$^{-/-}$ macrophages (Figure 3a–d).

We further validated increased SYK phosphorylation following knockout of CD33 using iPSdMiG. Next to CD33$^{-/-}$ iPSdMiG, we included the AD-protective CD33 variant CD33^{ΔE2} (Exon 2-spliced CD33) expressing iPSdMiG. IPSdMiG were obtained through differentiation of WT and isogenic CD33$^{-/-}$ as well as CD33^{ΔE2} iPSCs. Flow cytometry analysis and semiquantitative real-time PCR confirmed that CD33$^{-/-}$ and CD33^{ΔE2} iPSdMiG lost surface expression of CD33 and gene transcription of full-length CD33, but CD33^{ΔE2} iPSdMiG showed high levels of CD33^{ΔE2} mRNA (Figure S1c–e). No difference in gene transcription of PTPN6 was observed (Figure S1f). In addition, all iPSdMiG lines were highly positive for myeloid markers CD11b, CD14, CD45, FcγRI and SIRPα indicating a pure microglia cell population (Figure S1g). SYK phosphorylation was assessed using the AlphaLISA technique, which is more sensitive than classical Western Blot and thus allows analysis of low input of material. UT CD33$^{-/-}$ and CD33^{ΔE2} iPSdMiG showed an increase in SYK phosphorylation compared to WT iPSdMiG (Figure 3e; WT 1.00 ± 0.08 compared to CD33$^{-/-}$ 1.56 ± 0.11 with p = .002 and CD33^{ΔE2} 1.43 ± 0.08 with p = .013). Stimulation of the iPSdMiG with an activating antibody against the ITAM-associated receptor TREM2 resulted in a pronounced increase in pSYK to tSYK ratio compared to isotype antibody-treated levels in all iPSdMiG lines (Figure 3f; WT from 1.00 ± 0.11 to 26.48 ± 5.05 with p = .036; CD33$^{-/-}$ from 1.95 ± 0.21 to 92.19 ± 8.45 with p < .001 and CD33^{ΔE2} from 1.31 ± 0.05 to 43.36 ± 5.95 with p < .001). Furthermore, TREM2 treatment sharply increased pSYK/tSYK levels in CD33$^{-/-}$ iPSdMiG compared to WT and CD33^{ΔE2} iPSdMiG (both p < .001). The moderate increase in pSYK/tSYK levels in CD33^{ΔE2} iPSdMiG following TREM2 stimulation was insignificant compared to WT iPSdMiG (p = .39). Interestingly, the mRNA levels of ITAM-containing TYROBP, which is upstream of SYK and ERK1/2 were elevated in CD33$^{-/-}$ and CD33^{ΔE2} iPSdMiG (Figure S1h). However, this upregulation was not seen in THP1 macrophages (Figure S1i).

In summary, deletion of CD33 and expression of CD33^{ΔE2} in iPSdMiG increased activatory signaling via increased phosphorylation of the kinases SYK and ERK1/2 in THP1 macrophages and iPSdMiG.

3.4 | Increased gene transcription of IL1B, IL8, and IL10 after CD33 knockout

Above, we demonstrated that the transcriptome profile changes in WT THP1 macrophages compared to CD33 knockout or to PTPN6 knockdown were predominantly associated with inflammation and cytokine/chemokine signaling-related pathways (Figure 2c). To confirm that knockout of CD33 or knockdown of PTPN6 (shPTPN6) in these cells results in cellular immune activation, we examined cytokine transcription in combination with LPS treatment in THP1 macrophages by qRT-PCR. Additionally, we analyzed the cytokine gene transcript levels of iPSdMiG differentiated from human CD33$^{-/-}$, CD33^{ΔE2} and isogenic control WT iPSCs by qRT-PCR.

In UT THP1 macrophages, gene transcription levels of TNFA were similar among all four cell lines (Figure 4a). In response to LPS stimulation, TNFA mRNA expression levels were increased (WT shCTRL from 1.00 ± 0.02 to 1.88 ± 0.18 with p < .001, WT shPTPN6 from 0.99 ± 0.04 to 1.54 ± 0.15 with p = .012, CD33$^{-/-}$ shCTRL from 0.90 ± 0.04 to 1.53 ± 0.11 with p = .002 and CD33$^{-/-}$ shPTPN6 from 0.74 ± 0.05 to 1.49 ± 0.06 with p < .001). However, TNFA gene transcription in LPS-treated THP1 macrophages was not affected by CD33 knockout or PTPN6 knockdown. Gene transcription levels of IL1B were constitutively increased in CD33$^{-/-}$ THP1 macrophages regardless of PTPN6 knockdown compared to WT shCTRL macrophages (Figure 4b; WT shCTRL 1.00 ± 0.07, CD33$^{-/-}$ shCTRL 3.83 ± 0.26 and CD33$^{-/-}$ shPTPN6 3.90 ± 0.34 with p < .001) and further enhanced after LPS treatment (WT shCTRL 2.06 ± 0.16, CD33$^{-/-}$ shCTRL 5.44 ± 0.25 and CD33$^{-/-}$ shPTPN6 4.75 ± 0.27 with p < .001). Likewise, constitutive IL8 mRNA levels were increased in UT CD33$^{-/-}$ THP1 macrophages (Figure 4c; WT shCTRL 1.00 ± 0.11 compared to CD33$^{-/-}$ shCTRL 2.96 ± 0.18, p < .001) and further elevated after LPS treatment (from 2.32 ± 0.17 to 4.81 ± 0.39, p < .001). Although PTPN6 knockdown did not affect IL8 gene transcription in WT THP1 macrophages, CD33$^{-/-}$ shPTPN6 cells exhibited a decrease in IL8 mRNA levels compared to CD33$^{-/-}$ shCTRL macrophages (CD33$^{-/-}$ shPTPN6 UT 1.54 ± 0.19 with p = .011 and 2.41 ± 0.44 after LPS treatment with p < .001, both compared to CD33$^{-/-}$ shCTRL). Next, we investigated gene transcription of the predominantly anti-inflammatory cytokine IL-10. CD33$^{-/-}$ shCTRL macrophages exhibited an increased constitutive IL10 mRNA transcription assessed by semiquantitative real-time PCR (Figure 4d; WT shCTRL 1.00 ± 0.04 compared to CD33$^{-/-}$ shCTRL 2.59 ± 0.58, p = .007). Although there was no significant difference between shCTRL and PTPN6 knockdown in WT THP1 macrophages, CD33$^{-/-}$ macrophages exhibited decreased IL10 mRNA transcripts after PTPN6 knockdown (CD33$^{-/-}$ shPTPN6 1.23 ± 0.16, p = .039). Similarly, LPS-treated THP1 macrophages with PTPN6 knockdown showed decreased IL10 gene transcription compared to controls (WT shCTRL 2.23 ± 0.26 compared to WT shPTPN6 0.60 ± 0.04, p = .005 and CD33$^{-/-}$ shCTRL 2.73 ± 0.44 compared to CD33$^{-/-}$ shPTPN6 1.40 ± 0.11, p = .048).

In addition, we analyzed inflammatory cytokine gene transcription in WT, CD33$^{-/-}$ and CD33^{ΔE2} iPSdMiG. Interestingly, iPSdMiG
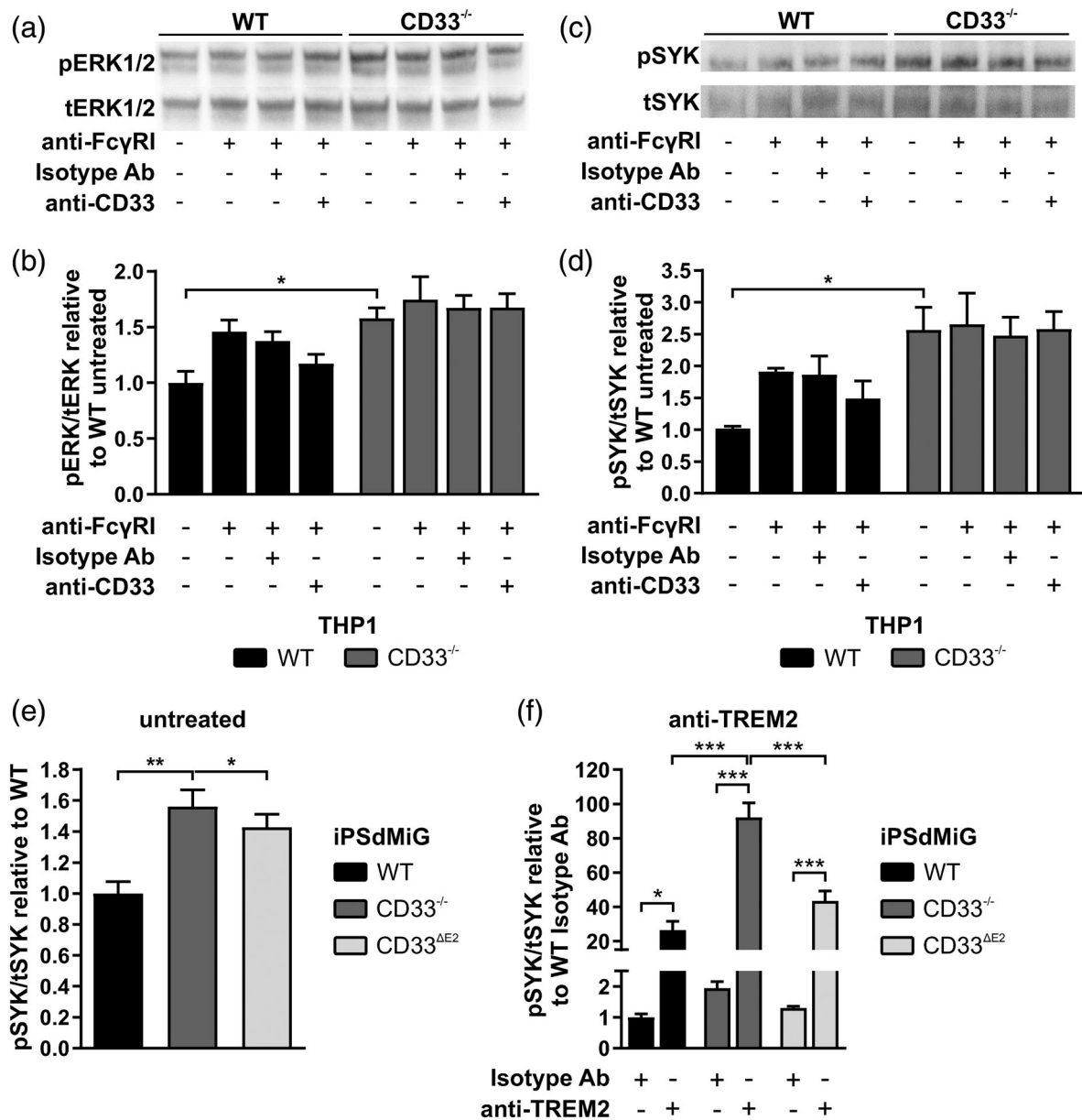
FIGURE 3 Activation of SYK and ERK1/2 signaling pathways as a consequence of *CD33* knockout in THP1 macrophages and human-induced pluripotent stem cell-derived microglia (iPSdMiG). (a) Western blot showing phosphorylated ERK1/2 (pERK1/2, top) and total ERK1/2 (tERK1/2, bottom) in wild type (WT) and CD33$^{-/-}$ macrophages. One representative image of five independent experiments is shown. (b) Quantification of pERK1/2 to tERK1/2 ratio in WT (black) and CD33$^{-/-}$ THP1 macrophages (dark gray). Knockout of *CD33* resulted in an increase in pERK1/2 in THP1 macrophages. FcγRI antibody treatment tended to increase pERK1/2 levels slightly in WT THP1 macrophages. CD33 antibody treatment following FcγRI antibody treatment tended to decrease the FcγRI antibody-driven increase in pERK1/2 to tERK1/2 levels only in WT THP1 macrophages. Data are shown as mean + SEM (n = 3–5). *$p \leq .05$ determined by two-way analysis of variance (ANOVA) followed by Bonferroni post hoc test. (c) Western blot showing phosphorylated SYK (pSYK, top) and total SYK (tSYK, bottom) in WT and CD33$^{-/-}$ macrophages. One representative image of three independent experiments is shown. (d) Quantification of pSYK to tSYK ratio in WT (black) and CD33$^{-/-}$ THP1 macrophages (dark gray). Knockout of *CD33* resulted in an increase in pSYK in THP1 macrophages. FcγRI antibody treatment tended to increase pSYK levels slightly and co-treatment with a CD33 antibody tended to counteract this increase, both only in WT THP1 macrophages. Data are shown as mean + SEM (n = 3). *$p \leq .05$ determined by two-way ANOVA followed by Bonferroni post hoc test. (e) SYK phosphorylation relative to total SYK assessed by AlphaLISA. Untreated iPSdMiG revealed an increased pSYK/tSYK ratio followed by knockout of *CD33* (dark gray) or expression of CD33$^{\Delta E2}$ (light gray) compared to WT iPSdMiG (black). Data are shown as mean + SEM (n = 6). **$p \leq .01$, *$p \leq .05$ determined by one-way ANOVA followed by Bonferroni post hoc test. (f) Treatment of iPSdMiG with activating antibodies for TREM2 resulted in an increased pSYK/tSYK ratio in WT (black), CD33$^{-/-}$ (dark gray) and CD33$^{\Delta E2}$ iPSdMiG (light gray) compared to isotype antibody-treated controls. Further, pSYK/tSYK was sharply increased in CD33$^{-/-}$ iPSdMiG following anti-TREM2 treatment. Data are shown as mean + SEM (n = 3). ***$p \leq .001$, *$p \leq .05$ determined by two-way ANOVA followed by Bonferroni post hoc test
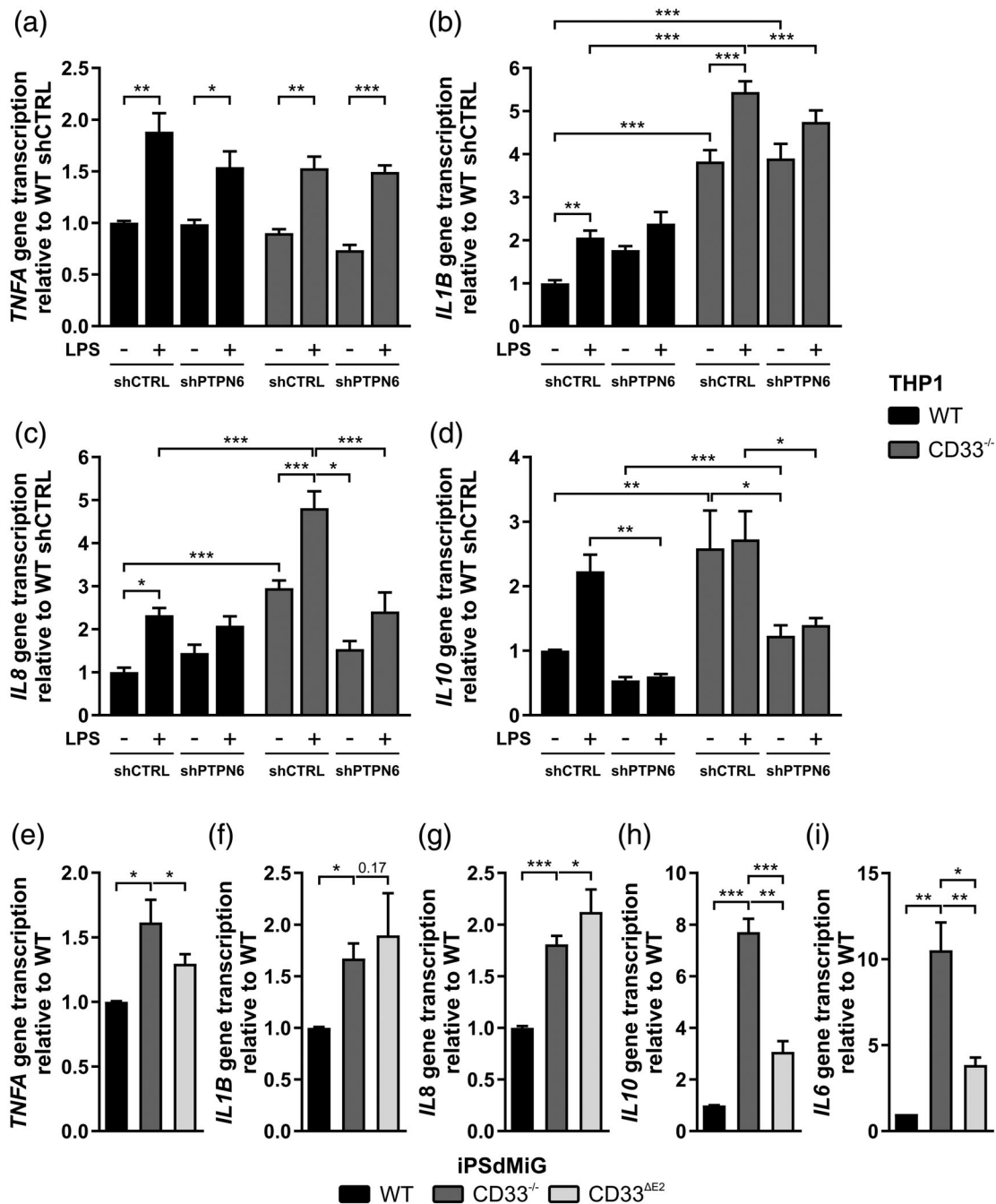
FIGURE 4 Inflammatory cytokine gene transcription is elevated after *CD33* knockout or *PTPN6* knockdown. (a) Semiquantitative real-time polymerase chain reaction (PCR) of *TNFA* gene transcription in THP1 macrophages. Gene transcription levels of *TNFA* were unchanged in untreated wild type (black) and CD33$^{-/-}$ (dark gray) THP1 macrophages regardless of *PTPN6* knockdown (shPTPN6). Following LPS treatment *TNFA* levels were increased. (b) *IL1B* mRNA levels in THP1 macrophages determined by semiquantitative real-time PCR. Knockout of *CD33* increased gene transcription of *IL1B* in THP1 macrophages (dark gray), which was further elevated by treatment with LPS. *IL1B* levels tended to be increased after *PTPN6* knockdown (shPTPN6) in wild-type THP1 macrophages (black). (c) *IL8* gene transcription in THP1 macrophages analyzed via semiquantitative real-time PCR. *IL8* mRNA levels were increased after knockout of *CD33* (dark gray) and elevated in all cell lines after LPS treatment. *PTPN6* knockdown (shPTPN6) attenuated the increase in *IL8* transcription in CD33$^{-/-}$ THP1 macrophages. (d) Semiquantitative real-time PCR of *IL10* mRNA levels in THP1 macrophages. Gene transcription levels of *IL10* were increased in CD33$^{-/-}$ THP1 macrophages (dark gray). Knockdown of *PTPN6* decreased *IL10* gene transcription below the control vector levels (shCTRL) in both, untreated and LPS-treated THP1 macrophages. Data are shown as mean + *SEM* (n = 3–7). ***$p \leq .001$, **$p \leq .01$, *$p \leq .05$ determined by two-way analysis of variance (ANOVA) followed by Bonferroni post hoc test. (e–i) Gene transcription levels of the inflammatory cytokines *TNFA, IL1B, IL8, IL10*, and *IL6* analyzed in wild type (WT) (black), CD33$^{-/-}$ (dark gray) and CD33$^{\Delta E2}$ human-induced pluripotent stem cell-derived microglia (iPSdMiG) (light gray) by semiquantitative real-time PCR. Knockout of *CD33* as well as expression of CD33$^{\Delta E2}$ in iPSdMiG resulted in constitutively elevated mRNA levels of (e) *TNFA*, (f) *IL1B*, (g) *IL8*, (h) *IL10*, and (i) *IL6*. *TNFA, IL10* and *IL6* mRNA levels were decreased in CD33$^{\Delta E2}$ iPSdMiG compared to CD33$^{-/-}$ iPSdMiG. Data are shown as mean + *SEM* (n = 5–6). ***$p \leq .001$, **$p \leq .01$, *$p \leq .05$ determined by Welch ANOVA followed by Games–Howell post hoc test

showed an increase in *TNFA* gene transcription after knockout of *CD33* (WT 1.00 ± 0.01 compared to CD33$^{-/-}$ 1.61 ± 0.18, *p* = .039) or in CD33^{ΔE2}-expressing iPSdMiG with lower magnitude (Figure 4e; CD33^{ΔE2} 1.29 ± 0.07, *p* = .024). In line with the THP1 macrophage data, increased *IL1B*, *IL8* and *IL10* gene transcript levels were observed in CD33$^{-/-}$ iPSdMiG (*IL1B* 1.00 ± 0.02–1.67 ± 0.15 with *p* = .021, *IL8* 1.00 ± 0.02–1.81 ± 0.08 with *p* < .001 and *IL10* 1.00 ± 0.00–7.71 ± 0.52 with *p* < .001; Figure 4f–h; WT vs. CD33$^{-/-}$, respectively). Furthermore, we analyzed the gene transcript levels of IL-6, which is known to play a critical role in chronic inflammation. *IL6* mRNA levels were sharply elevated in CD33$^{-/-}$ iPSdMiG compared to WT control iPSdMiG (Figure 4i; 1.00 ± 0.00–10.52 ± 1.62, *p* = .005). CD33^{ΔE2}-expressing iPSdMiG showed a similar trend than CD33$^{-/-}$ iPSdMiG regarding *IL1B* and *IL8* gene transcription levels (Figure 4f; 1.98 ± 0.41, *p* = .168 and Figure 4g; 2.12 ± 0.22, *p* = .014). *IL10* and *IL6* mRNA levels, however, were increased compared to WT iPSdMiG but much lower compared to CD33$^{-/-}$ iPSdMiG (Figure 4h; 3.07 ± 0.41, *p* = .009 compared to WT and *p* < .001 compared to CD33$^{-/-}$ and Figure 4i; 3.85 ± 0.43, *p* = .003 compared to WT and *p* = .019 compared to CD33$^{-/-}$).

In line with the transcriptome data, inflammatory cytokine gene transcription analyzed by qRT-PCR was increased in CD33$^{-/-}$ THP1 macrophages and CD33$^{-/-}$ as well as CD33^{ΔE2} iPSdMiG. In addition, the LPS-induced increase in *IL10* gene transcription was dependent on CD33 and SHP1 (*PTPN6*).

3.5 | Increased gene transcription of the AD-associated phosphatase INPP5D after *CD33* knockout and *PTPN6* knockdown

Cells often use compensatory mechanisms to counteract the loss of a specific protein or pathway, which is known as genetic compensation response. In order to address whether there is a compensatory upregulation of other inhibitory signaling pathways following *CD33* knockout or *PTPN6* knockdown, we analyzed the expression of the ITIM-bearing receptor SIRP-α (*SIRPA*) and the ITIM signaling-associated phosphatases *PTPN11*/SHP2 and *INPP5D*/SHIP1 via qRT-PCR. *SIRPA* gene transcription was increased in *CD33* knockout and *PTPN6* knockdown THP1 macrophages (Figure 5a; WT shCTRL 1.00 ± 0.03, WT shPTPN6 2.11 ± 0.06 with *p* = .013, CD33$^{-/-}$ shCTRL 2.72 ± 0.25 with *p* < .001 and CD33$^{-/-}$ shPTPN6 3.32 ± 0.34 with *p* < .001), but this upregulation was not significant in *CD33*-deficient iPSdMiG and absent in CD33^{ΔE2} iPSdMiG as demonstrated by qRT-PCR (Figure 5b; WT 1.00 ± 0.00, CD33$^{-/-}$ 1.59 ± 0.25 with *p* = .15 and CD33^{ΔE2} 1.13 ± 0.11). Gene transcription of *PTPN11* was elevated in CD33$^{-/-}$ THP1 macrophages (Figure 5c; WT shCTRL 1.00 ± 0.05, CD33$^{-/-}$ shCTRL 2.75 ± 0.15 with *p* < .001 and CD33$^{-/-}$ shPTPN6 1.95 ± 0.09 with *p* = .006), but remained unchanged in iPSdMiG (Figure 5d). Only *INPP5D* mRNA levels were upregulated following knockout of *CD33* in both, THP1 macrophages (Figure 5e; WT shCTRL 1.00 ± 0.04, CD33$^{-/-}$ shCTRL 2.60 ± 0.13 with *p* = .001 and CD33$^{-/-}$ shPTPN6 2.61 ± 0.26 with *p* = .001) and iPSdMiG

(Figure 5f; WT 1.00 ± 0.00 compared to CD33$^{-/-}$ 1.71 ± 0.11, *p* = .003). Interestingly, CD33^{ΔE2} iPSdMiG also showed a slight upregulation of *INPP5D* transcripts (1.23 ± 0.06 with *p* = .032 compared to WT and *p* = .016 compared to CD33$^{-/-}$).

Thus, knockout of *CD33* led to increased gene transcription of the phosphatase *INPP5D* (*SHIP1*) in THP1 macrophages and iPSdMiG.

3.6 | Increased phagocytosis and phagocytosis-associated oxidative burst after deletion of *CD33*

Phagocytosis is a tightly regulated key competence of macrophages and microglia. To test whether knockout of *CD33* or expression of AD-protective CD33^{ΔE2} also influences phagocytosis, we challenged THP1 macrophages and iPSdMiG with pHrodo-conjugated *S. aureus* BioParticles. Bacterial peptidoglycans and lipoteichoic acid of the cell wall of *S. aureus* are recognized by innate immune receptors and consequently phagocytosed. After phagocytic uptake and fusion of the phagosome with an acidic lysosome, the pH-sensitive pHrodo dye will become fluorescent. THP1 macrophages with *PTPN6* knockdown (WT shPTPN6) as well as CD33$^{-/-}$ shCTRL and CD33$^{-/-}$ shPTPN6 macrophages showed increased pHrodo *S. aureus* phagocytosis compared to WT shCTRL THP1 macrophages (Figure 6a,b; WT shCTRL 1.00 ± 0.09, WT shPTPN6 2.28 ± 0.24 with *p* = .01, CD33$^{-/-}$ shCTRL 2.12 ± 0.34 with *p* = .024 and CD33$^{-/-}$ shPTPN6 2.02 ± 0.14 with *p* = .042). Likewise, CD33$^{-/-}$ but also CD33^{ΔE2}-expressing iPSdMiG showed an increase in pHrodo BioParticles phagocytosis compared to WT cells (Figure 6c,d; WT 1.00 ± 0.21 compared to CD33$^{-/-}$ 2.37 ± 0.12 with *p* < .001 and CD33^{ΔE2} 1.96 ± 0.15 with *p* = .008).

Next, we challenged THP1 macrophages and iPSdMiG with aggregated Aβ$_{1-42}$ to study their response to a noninfectious disease-related stimulus. Phagocytosis of Aβ$_{1-42}$ was detected by co-staining of Aβ$_{1-42}$ with CD11b or IBA1 (Figure 6e,g). The uptake of Aβ$_{1-42}$ was enhanced in WT shPTPN6 as well as in CD33$^{-/-}$ shCTRL and shPTPN6 THP1 macrophages compared to WT shCTRL THP1 macrophages. (Figure 6f; WT shCTRL 1.00 ± 0.04, WT shPTPN6 1.78 ± 0.07, CD33$^{-/-}$ shCTRL 1.82 ± 0.04 and CD33$^{-/-}$ shPTPN6 1.80 ± 0.07, all *p* < .001 compared to WT shCTRL). Similarly, phagocytosis of fluorescent cellular debris counterstained with CD11b (Figure S3a) was increased after knockout of *CD33* or knockdown of *PTPN6* in THP1 macrophages (Figure S3b; WT shCTRL 1.00 ± 0.05; WT shPTPN6 2.04 ± 0.09; CD33$^{-/-}$ shCTRL 2.07 ± 0.08; CD33$^{-/-}$ shPTPN6 2.01 ± 0.05 with *p* < .001). In line with these findings, CD33$^{-/-}$ as well as CD33^{ΔE2}-expressing iPSdMiG exhibited an increase in uptake of aggregated Aβ$_{1-42}$ compared to the corresponding WT control iPSdMiG (Figure 6g,h; WT 1.00 ± 0.08 compared to CD33$^{-/-}$ 1.67 ± 0.11 with *p* = .001 and CD33^{ΔE2} 1.42 ± 0.06 with *p* = .021).

Phagocytosis of bacteria, debris or aggregated proteins is often accompanied by release of radicals as oxidative burst throughout the phagocytic process. Therefore, we examined the radical production induced by treatment with aggregated Aβ$_{1-42}$ in THP1 macrophages

FIGURE 5 Increased gene transcription of *INPP5D* (*SHIP1*) caused by loss of *CD33*.(a + b) Gene transcription of *SIRPA* measured by semiquantitative real-time polymerase chain reaction (qRT-PCR). *SIRPA* mRNA levels were increased in CD33$^{-/-}$ (dark gray) and *PTPN6* knockdown (shPTPN6) wild type (WT) THP1 macrophages (black). *PTPN6* knockdown in CD33$^{-/-}$ macrophages further enhanced this effect. However, in human-induced pluripotent stem cell-derived microglia (iPSdMiG) *SIRPA* transcription only tended to be increased after knockout of CD33 and remained unchanged in CD33$^{\Delta E2}$ iPSdMiG. (c + d) *PTPN11* (*SHP2*) mRNA levels analyzed via semiquantitative real-time PCR. *PTPN11* gene transcripts were increased in CD33$^{-/-}$ (dark gray) THP1 macrophages. Knockdown of *PTPN6* in CD33$^{-/-}$ macrophages resulted in a slightly dampened increase in *PTPN11* gene transcription. iPSdMiG exhibited no change in *PTPN11* transcription after knockout of *CD33* or in CD33$^{\Delta E2}$-expressing iPSdMiG. (e + f) Semiquantitative real-time PCR of CD33 adapter molecule *INPP5D* (*SHIP1*) in THP1 macrophages and iPSdMiG. Knockout of *CD33* (dark gray) increased *INPP5D* mRNA levels compared to WT THP1 macrophages (black) regardless of *PTPN6* knockdown. Similarly, *INPP5D* gene transcription was elevated in CD33$^{-/-}$ iPSdMiG and to lesser extend in CD33$^{\Delta E2}$ iPSdMiG. Data are shown as mean + *SEM* (*n* = 3–6). ***p ≤ .001, **p ≤ .01, *p ≤ .05 determined by two-way analysis of variance (ANOVA) followed by Bonferroni post hoc test (THP1) or Welch ANOVA followed by Games–Howell post hoc test (iPSdMiG)
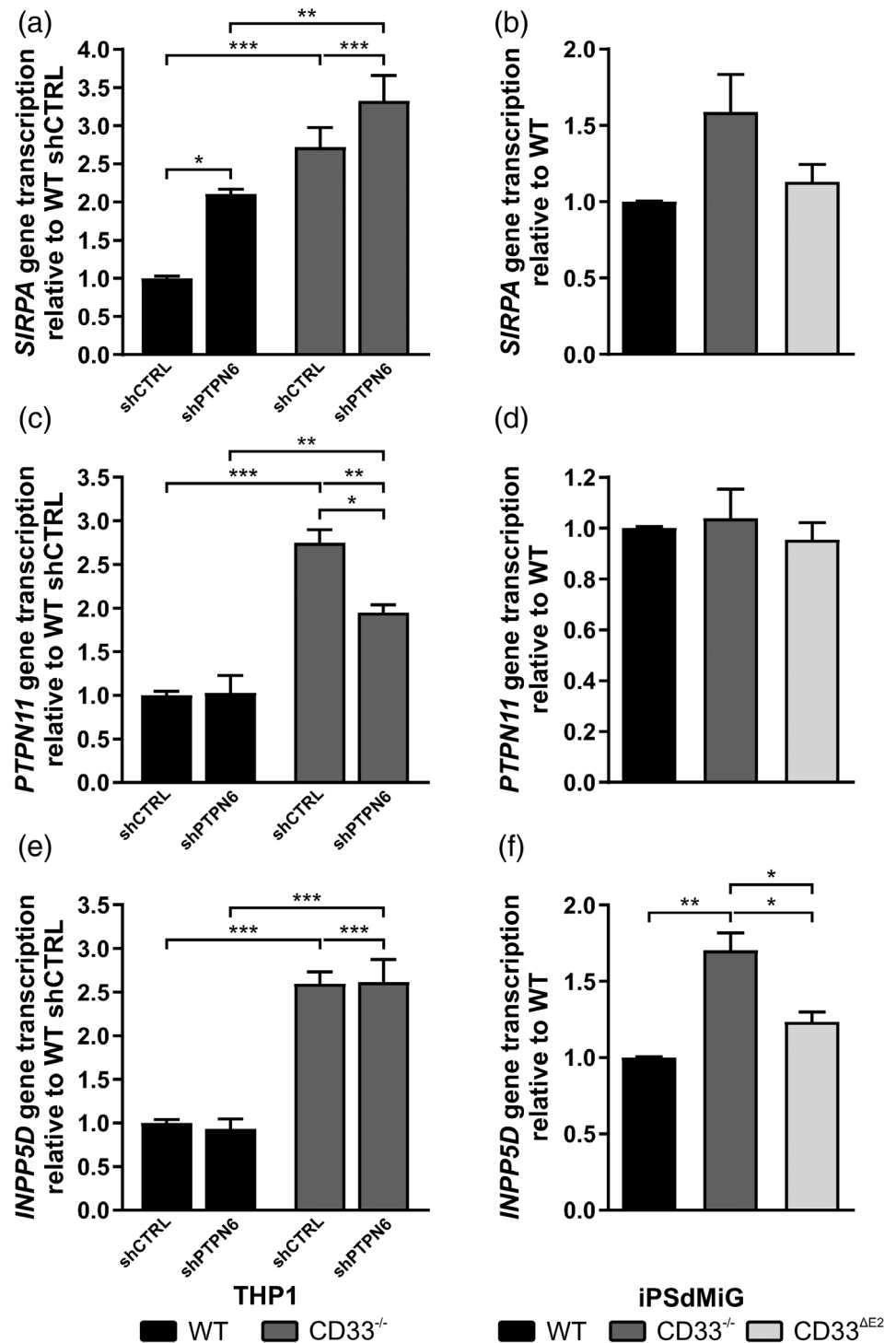
and *S. aureus* BioParticles in iPSdMiG via staining with the oxidation-sensitive fluorescent dye DHE. Thereby, the constitutive DHE fluorescent intensity as read-out of basal radical production in UT cells did not vary in the four different THP1 macrophage cell lines, irrespective of *CD33* knockout or *PTPN6* knockdown. However, in response to acute exposure to Aβ$_{1-42}$, CD33$^{-/-}$ shCTRL THP1 macrophages released higher amounts of radicals (Figure 7a; 2.13 ± 0.12) in comparison to WT shCTRL THP1 macrophages (1.54 ± 0.06, p = .006) indicated by increased DHE staining. Treatment with SOD1 or Trolox,

which are radical scavengers, attenuated the increased oxidative burst to the levels of UT cells (Figure 7a). Challenging THP1 macrophages with cellular debris increased radical production in all cell lines compared to the UT controls. Moreover, knockout of *CD33* resulted in a further elevation of radical production regardless of *PTPN6* knockdown (Supplementary Figure S3c; WT shCTRL 1.56 ± 0.05, CD33$^{-/-}$ shCTRL 1.99 ± 0.08 with p = .018 and CD33$^{-/-}$ shPTPN6 1.98 ± 0.12 with p = .026). Again, the oxidative burst triggered by cellular debris was reduced by pretreatment of the cells with the radical scavengers

SOD1 or Trolox in all experimental groups, respectively (Supplementary Figure S3c). In line with the THP1 data, constitutive reactive oxygen production did not vary between WT, CD33$^{-/-}$ and CD33$^{\Delta E2}$ iPSdMiG (Figure 7b; WT UT 1.00 ± 0.05 compared to CD33$^{-/-}$ UT 1.11 ± 0.06 and CD33$^{\Delta E2}$ UT 0.89 ± 0.09). Treatment of iPSdMiG with nonlabeled *S. aureus* BioParticles increased radical production in all iPSdMiG lines (WT BioParticles 1.47 ± 0.06 with *p* = .002; CD33$^{-/-}$ BioParticles 2.02 ± 0.11 with *p* < .001 and CD33$^{\Delta E2}$ BioParticles 1.36 ± 0.05 with *p* = .11) with a higher magnitude in CD33$^{-/-}$ iPSdMiG (*p* ≤ .001 compared to WT and CD33$^{\Delta E2}$ BioParticles-treated iPSdMiG). Treatment with the antioxidant NAC successfully attenuated the BioParticles-induced ROS production.

Thus, deficiency of *CD33* and knockdown of *PTPN6* caused increased phagocytosis and phagocytosis-associated oxidative burst in THP1 macrophages as well as in iPSdMiG. However, expression of CD33$^{\Delta E2}$ in iPSdMiG only led to upregulation of phagocytosis but not of the associated oxidative burst.
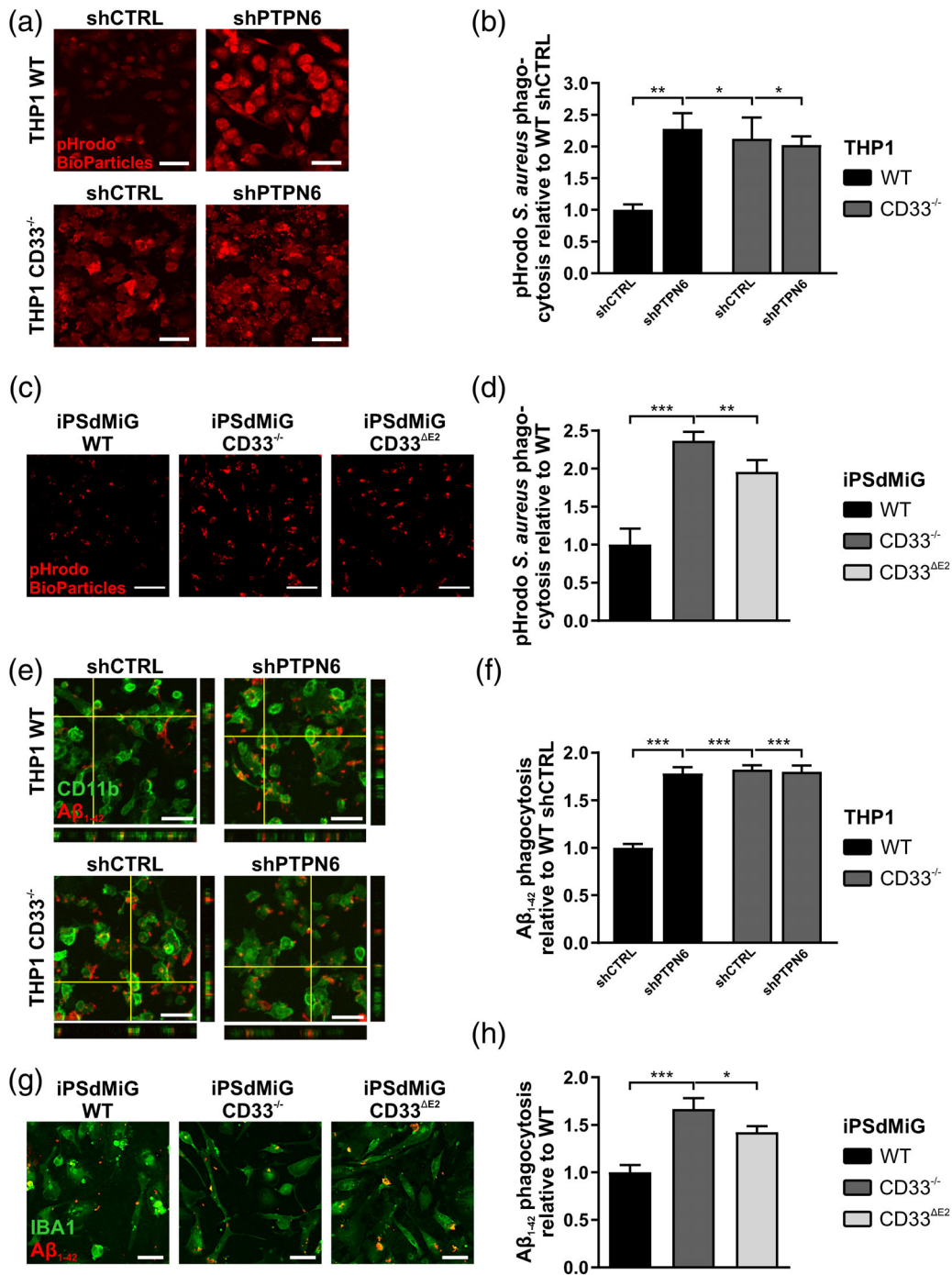

FIGURE 6 Legend on next page.

4 | DISCUSSION

Several recent studies linked polymorphisms in the *CD33* gene to AD, thereby creating a need to understand the function of CD33 in human microglia. Human CD33 has been postulated to have physiological endocytic properties for recycling sialylated antigens (Walter et al., 2008). Furthermore, in brains of AD patients, CD33 protein levels as well as the number of CD33^{+} microglia are upregulated, and positively correlate with increased Aβ plaque load (Bradshaw et al., 2013; Griciuc et al., 2013). Two co-inherited SNPs in the Caucasian population (rs3865444(A/A) and rs12459419(T/T)) are associated with decreased CD33 surface expression and expression of the Exon 2-deleted isoform of CD33 (D2-CD33/CD33[ΔE2]). In addition, rs3865444(A/A) is associated with an overall decreased odds ratio to develop AD (Hollingworth et al., 2011; Naj et al., 2011). However, the exact role of CD33 in the brain in health and disease is still not fully understood. In this study, we determined the effects of expression of CD33[ΔE2] or loss of CD33 in conjunction with knockdown of one of its downstream signaling molecules PTPN6/SHP1 in human macrophages and microglia. Mice have no direct orthologue of human CD33, since mouse CD33 lacks the typical ITIM signaling domain and has a charged residue, which might allow binding to the activatory membrane molecule TYROBP/DAP12 (Brinkman-Van der Linden et al., 2003). Indeed, it was shown that surface expression of mouse CD33 is stabilized by interaction with TYROBP (Bhattacherjee et al., 2019). Thus, CD33^{−/−} mice appear to be unsuitable as model system for the functional analysis of human CD33. For this reason, we used human CD33^{−/−} THP1 macrophages and human CD33^{−/−} or CD33[ΔE2]-expressing iPSdMiG, which are microglia derived from human iPSCs and compared them to their WT counterparts as in vitro model systems.

In line with recent findings, the Exon 2-deleted isoform of CD33, CD33[ΔE2], was not detected on the cell surface by flow cytometry with an anti-CD33 antibody clone targeting the C2 domain, which is in theory able to detect CD33[ΔE2] (Siddiqui et al., 2017). Human CD33 mediates inhibitory signaling via its intracellular ITIM domain, which acts as a counterpart of ITAMs. Therefore, we analyzed the phosphorylation status of downstream molecules of the ITAM signaling pathway, namely SYK and ERK1/2, via Western blot or AlphaLISA. CD33^{−/−} THP1 macrophages exhibited a higher ratio of pSYK to tSYK and pERK1/2 to tERK1/2 in comparison to WT control macrophages. Activation of FcγRI via a cross-linking antibody tended to increase phosphorylation of SYK and ERK1/2 in WT macrophages. However, CD33^{−/−} macrophages clearly did not show any tendency for increased pSYK or pERK1/2 after cross-linking of FcγRI. Similarly, cross-linking of CD33 slightly reduced pSYK and pERK1/2 levels in WT macrophages, but not in CD33^{−/−} macrophages. In line, UT CD33^{−/−} and CD33[ΔE2] iPSdMiG showed increased pSYK/tSYK levels compared to WT iPSdMiG. Further, activation of TREM2 via cross-linking antibodies increased the pSYK/tSYK ratio in CD33^{−/−} iPSdMiG compared WT and CD33[ΔE2] iPSdMiG, suggesting an impaired ability to counteract the increased ITAM signaling after deletion of *CD33*, but not in CD33[ΔE2]-expressing iPSdMiG. Thus, lack of inhibitory CD33 signaling causes an imbalance in the ITIM-ITAM signaling axis toward increased ITAM signaling. However, increased SYK and ERK1/2 signaling in macrophages and microglia could also lead to increased proliferation and survival as well as a beneficial immune response against disease-associated triggers (Callaway et al., 2015; Crowley et al., 1997).

A previous study showed that human monocytes produce the pro-inflammatory cytokines TNF-α, IL-1β, and IL-8 after blocking CD33 signaling with an antibody as well as by *CD33* siRNA treatment (Lajaunias, Dayer, & Chizzolini, 2005). In addition, it has been reported that desialylation of THP1 macrophages also increases IL-8 secretion in a CD33-dependent manner (Zaric et al., 2017). In line with these results, CD33^{−/−} shCTRL THP1 macrophages and CD33^{−/−} as well as CD33[ΔE2] iPSdMiG exhibited an increase in *IL1B*, *IL8* and *IL10* mRNA levels. Interestingly, the magnitude of increased gene transcription of

FIGURE 6 Increased phagocytosis of pHrodo-labeled bacterial particles and aggregated amyloid β$_{1-42}$ (Aβ$_{1-42}$) in *CD33* knockout and *PTPN6* knockdown phagocytes. (a) Confocal images showing phagocytosed pHrodo *Staphylococcus aureus* BioParticles in wild type (WT) and CD33^{−/−} THP1 macrophages. The phagocytes were incubated with 1 mg/ml bacterial particles for 120 min. Scale bar = 50 μm. (b) Quantification of the bacterial particle intensities in THP1 macrophages. *CD33* knockout (dark gray) as well as *PTPN6* knockdown (shPTPN6) cells demonstrated an increase in phagocytosis compared to the wild-type control (black). Data are shown as mean + *SEM* (n = 4). **p ≤ .01, *p ≤ .05 determined by two-way analysis of variance (ANOVA) followed by Bonferroni post hoc test. (c) Live cell images showing pHrodo *S. aureus* BioParticles in WT, CD33^{−/−} and CD33[ΔE2] human-induced pluripotent stem cell-derived microglia (iPSdMiG). The phagocytes were incubated with 0.5 mg/ml bacterial particles for 90 min. Scale bar = 100 μm. (d) Likewise, CD33^{−/−} (dark gray) as well as CD33[ΔE2] (light gray) iPSdMiG exhibited an increased *S. aureus* BioParticle phagocytosis compared to the corresponding wildtype control cells (black). Data are shown as mean + *SEM* (n = 4). ***p ≤ .001, **p ≤ .01 determined by one-way ANOVA followed by Bonferroni post hoc test. (e) Phagocytosis of aggregated Aβ$_{1-42}$ by WT and CD33^{−/−} THP1 macrophages. Macrophages were identified by CD11b staining (green) and the phagocytosed fluorescent Aβ$_{1-42}$ (red) was detected inside the cells by z-stack images. Scale bar = 50 μm. (f) Quantification of Aβ$_{1-42}$ phagocytosis as the ratio of the number of Aβ$_{1-42}$[+] macrophages to the total number of macrophages. CD33^{−/−} (dark gray) as well as *PTPN6* knockdown (shPTPN6) THP1 macrophages exhibited an increase in Aβ$_{1-42}$ uptake. Data are shown as mean + *SEM* (n = 4). ***p ≤ .001 determined by two-way ANOVA followed by Bonferroni post hoc test. (g) Phagocytosis of aggregated Aβ$_{1-42}$ by WT, CD33^{−/−} and CD33[ΔE2] iPSdMiG. iPSdMiG were identified by IBA1 staining (green) and the phagocytosed fluorescent Aβ$_{1-42}$ (red) was detected inside the cells by z-stack images. Scale bar = 50 μm. (h) Quantification of relative Aβ$_{1-42}$ phagocytosis in iPSdMiG. CD33^{−/−} (dark gray) as well as CD33[ΔE2] (light gray) iPSdMiG showed an increased Aβ$_{1-42}$ phagocytosis compared to the corresponding wildtype control cells (black). Data are shown as mean + *SEM* (n = 4). ***p ≤ .001, **p ≤ .01, *p ≤ .05 determined by one-way ANOVA followed by Bonferroni post hoc test
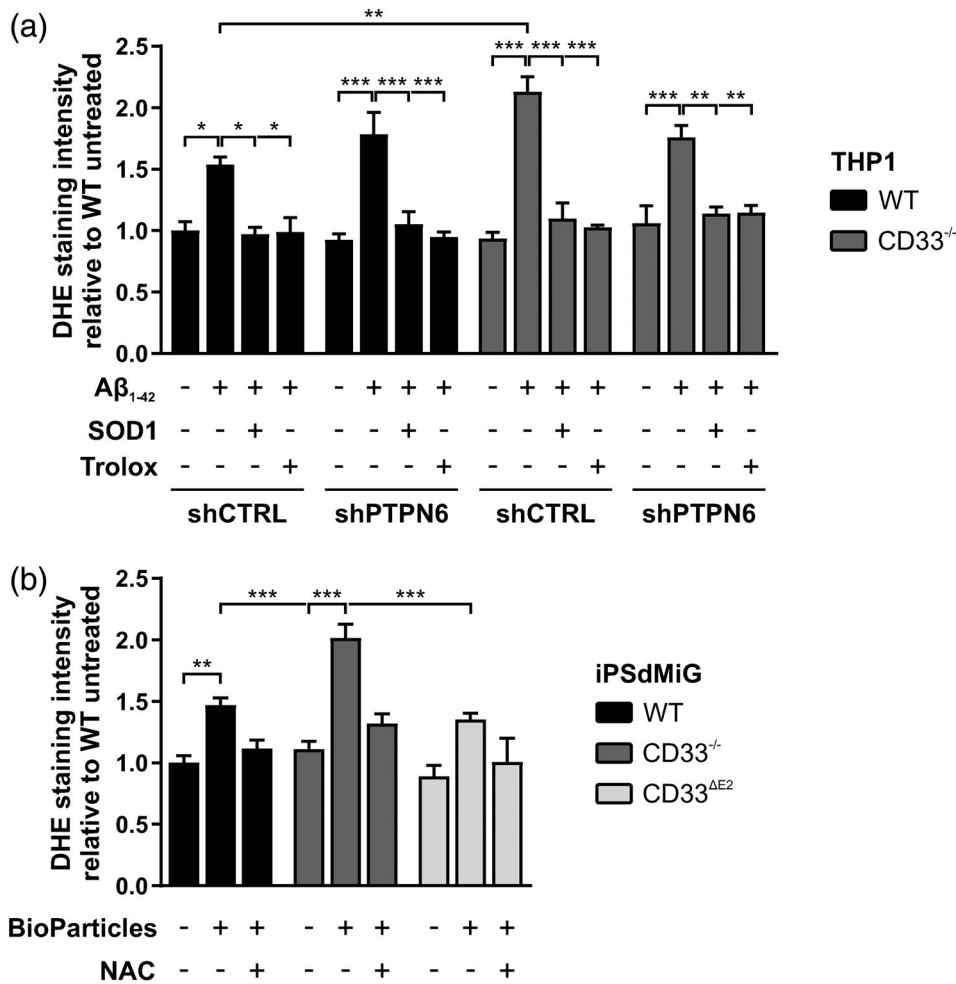
FIGURE 7 Knockout of *CD33* increased radical production in human macrophages and microglia. (a) Production of radicals in THP1 macrophages was assessed by dihydroethidium (DHE) staining and confocal microscopy. Radical production was increased by $A\beta_{1-42}$ in all four cell lines indicated by DHE staining intensity. Thereby, $A\beta_{1-42}$-induced radical production in $CD33^{-/-}$ shCTRL macrophages (dark gray) was enhanced compared to the corresponding wild-type (black) shCTRL line. Treatment with scavengers SOD1 and Trolox attenuated the $A\beta_{1-42}$-driven effect to untreated levels. Data are shown as mean + *SEM* (*n* = 4). ***p ≤ .001, **p ≤ .01, *p ≤ .05 determined by two-way analysis of variance (ANOVA) followed by Bonferroni post hoc test. (b) Reactive oxygen species (ROS) production in human-induced pluripotent stem cell-derived microglia (iPSdMiG) analyzed by DHE staining. Wild type (WT) (black), $CD33^{-/-}$ (dark gray) and $CD33^{\Delta E2}$ (light gray) iPSdMiG exhibited similar constitutive ROS production. Treatment of the phagocytes with bacterial particles from *S. aureus* resulted in an elevated production of ROS in all iPSdMiG lines with a higher magnitude in $CD33^{-/-}$ iPSdMiG. Treatment with the scavenger NAC decreased ROS production to untreated levels. Data are shown as mean + *SEM* (*n* = 3–6). ***p ≤ .001, **p ≤ .01 determined by two-way ANOVA followed by Bonferroni post hoc test

IL6 and *IL10* was higher in $CD33^{-/-}$ iPSdMiG compared to $CD33^{\Delta E2}$ iPSdMiG, suggesting only a partial loss of inhibitory CD33 signaling in $CD33^{\Delta E2}$-expressing iPSdMiG. The increased gene transcripts of the anti-inflammatory cytokine *IL10* in $CD33^{-/-}$ and $CD33^{\Delta E2}$ iPSdMiG as well as $CD33^{-/-}$ THP1 macrophages might act as counter-regulator of the increased pro-inflammatory gene transcripts *IL1B* and *IL8*, thus keeping the net outcome on inflammation unclear. Knockdown of *PTPN6* did not influence gene transcription levels of *TNFA* compared to controls in both, UT and LPS-treated WT THP1. However, *IL1B* levels tended to be increased by around twofold on transcription level in UT WT macrophages after *PTPN6* knockdown. Bone marrow-derived macrophages (BMDM) isolated from motheaten viable mice with reduced *PTPN6*/SHP1 expression showed an increase in TNF-α production after

LPS treatment compared to BMDM from WT mice, but no change in IL-1β production after LPS stimulation (Rego et al., 2011). The difference between the report by Rego et al. (2011) and our results could have a multitude of reasons such as timing of the analyses, cell type or species differences. The gene transcription of *IL10* was suppressed in LPS-treated WT and $CD33^{-/-}$ THP1 macrophages after *PTPN6* knockdown compared to the control (shCTRL). Likewise, *IL10* gene transcription was suppressed in BMDM from motheaten viable mice after LPS treatment (Okenwa et al., 2013), which suggests that PTPN6/SHP1 positively regulates production of IL-10. Furthermore, *IL8* mRNA levels were also decreased in $CD33^{-/-}$ macrophages after *PTPN6* knockdown regardless of LPS treatment, which indicates regulation of *IL8* gene transcription through PTPN6/SHP1 in a CD33-dependent manner.

Lack of CD33 signaling might influence the expression of other ITIM-bearing receptors or associated downstream molecules. Therefore, we examined mRNA levels of *SIRPA*/SIRP-α, *PTPN11*/SHP2, and *INPP5D*/SHIP1. SIRP-α exerts its inhibitory effect on phagocytosis, when it interacts with CD47. Engagement of CD47 causes phosphorylation of the ITIM of SIRP-α, which results in the recruitment and activation of SHP1 or SHP2 and thus in decreased phagocytosis (Matozaki, Murata, Okazawa, & Ohnishi, 2009; Neznanov et al., 2003). Our data demonstrate an increase of *SIRPA* mRNA levels after *PTPN6* knockdown or *CD33* knockout in THP1 macrophages, but only a tendency for increase in CD33$^{-/-}$ iPSdMiG and no effect in CD33$^{\Delta E2}$-expressing iPSdMiG, suggesting differences of CD33 function in the distinct cell types. Additionally, the inhibitory signaling phosphatases, *PTPN11* and *INPP5D*, were upregulated in CD33$^{-/-}$ THP1 macrophages on transcription level. This upregulation was also seen in CD33$^{-/-}$ iPSdMiG for *INPP5D*. Thus, deletion of *CD33* as a major ITIM-bearing receptor might cause compensatory upregulation of other ITIM-associated phosphatases as shown for INPP5D/SHIP1. Interestingly, polymorphisms in the phosphatase INPP5D/SHIP1 gene have been also associated with AD (Lambert et al., 2013).

Moreover, previous studies indicated that the level of CD33 expression is positively correlated with Aβ load in the human brain and inversely associated with microglial phagocytic ability (Bradshaw et al., 2013; Griciuc et al., 2013). Further, PTPN6/SHP1 overexpression in J774A.1 macrophages results in a complete diminished phagocytosis of IgG-sensitized sheep red blood cells (Kant et al., 2002), and the phagocytic capacity of neonatal macrophages is negatively correlated to PTPN6/SHP1 activity (Lawrence & Koenig, 2012). In addition to these publications, our study now shows that CD33$^{-/-}$ and CD33$^{\Delta E2}$-expressing iPSdMiG as well as CD33$^{-/-}$ THP1 macrophages and WT THP1 macrophages with *PTPN6* knockdown exhibited an increased phagocytosis of bacterial particles and aggregated Aβ$_{1-42}$. The production of ROS such as superoxide during the phagocytosis-associated oxidative burst is another hallmark of macrophages and microglia and essential for the host defense against microorganisms. The oxidative burst is tightly controlled in order to prevent host tissue damage. TYROBP-mediated ITAM signaling activates the nicotinamide adenine dinucleotide phosphate oxidase NOX2 to produce ROS (Graham et al., 2007). It was shown that murine Siglec-E as well as human SIGLEC-11, which show similar inhibitory signaling function to human CD33, inhibit the phagocytosis and the phagocytosis-associated oxidative burst (Claude, Linnartz-Gerlach, Kudin, Kunz, & Neumann, 2013; Shahraz et al., 2015; Wang & Neumann, 2010). In our current study, neither knockout of *CD33* nor expression of CD33$^{\Delta E2}$ in iPSdMiG induced an increase in constitutive ROS production. However, CD33 deficiency enhanced phagocytosis-associated oxidative burst in THP1 shCTRL macrophages after treatment with Aβ$_{1-42}$ or cellular debris. In line, CD33$^{-/-}$ but not CD33$^{\Delta E2}$ iPSdMiG showed increased phagocytosis-associated ROS production following *S. aureus* BioParticles treatment. Interestingly, recent studies showed that the AD-protective

variant CD33$^{\Delta E2}$ is localized in peroxisomes, and it is speculated that CD33$^{\Delta E2}$ is related to peroxisome proliferation as well as ROS metabolism and thereby has a protective effect, which a knockout of *CD33* does not show (Siddiqui et al., 2017). Similar to CD33-related SIGLECs, PTPN6/SHP1 is also known as a negative regulator of ROS production in various cells types (Gruber et al., 2015; Krotz et al., 2005; Lyons et al., 2003). In our results, *PTPN6* knockdown only showed a slight increase in ROS production after stimulation with Aβ$_{1-42}$ or cellular debris in WT macrophages, which might be attributed to the partial loss of PTPN6/SHP1 signaling. However, ROS production was slightly dampened in CD33$^{-/-}$ macrophages with *PTPN6* knockdown. Increased SYK/ERK1/2 signaling in conjunction with increased phagocytosis could be a sign of a productive immune response, which might be beneficial in diseases such as AD. However, in combination with increased inflammatory cytokine/chemokine signaling and phagocytic oxidative burst as seen for knockout of *CD33* in human THP1 macrophages and iPSdMiG proinflammatory activation of the phagocytes might result in collateral damage to neighboring cells such as neurons.

In summary, our data demonstrate that deletion of *CD33* and knockdown of *PTPN6* only in WT but not in CD33$^{-/-}$ background lead to immune activation of human macrophages and microglia, probably through the SYK-ERK signaling axis. Interestingly, expression of CD33$^{\Delta E2}$ in iPSdMiG shows a dampened activatory phenotype without increased phagocytic oxidative burst compared to a full *CD33* knockout, suggesting only a partial loss of inhibitory CD33 signaling and absence of the potentially toxic oxidative burst associated with phagocytosis. Further, knockout of *CD33* is accompanied by gene transcript upregulation of the ITIM-associated phosphatase *INPP5D*, which was also shown to be associated with AD. In addition, our study demonstrates that loss of inhibitory signaling via knockout of *CD33*, expression of CD33$^{\Delta E2}$ or knockdown of *PTPN6* results in increased phagocytosis of aggregated Aβ$_{1-42}$, cellular debris and bacterial particles. Thus, CD33 as well as PTPN6/SHP1 may be potential pharmacological targets for inducing a productive immune response to clear off Aβ plaques in AD. On the other hand, ablating CD33 signaling in the brain may be a double-edged sword as loss of CD33, but not expression of CD33$^{\Delta E2}$, might increase the potentially detrimental phagocytosis-associated oxidative burst.

ART: SMART was used to create the table of content image under the license agreement creativecommons.org/licenses/by/3.0/deed.en. Open Access funding enabled and organized by ProjektDEAL. WOA Institution: RHEINISCHE FRIEDRICH-WILHELMS-UNIVERSITAET BONN. Blended DEAL: ProjektDEAL.

CONFLICT OF INTERESTS

M. M. and O. B. are named inventors of a submitted patent related to upscaled production of iPSC-derived microglia and macrophages (EP20162230) that is assigned to the LIFE & BRAIN GmbH. O. B. and H. N. are named inventors on a patent related to generation of microglial precursors from pluripotent stem cells (patent family to WO2010125110A1) that is assigned to the LIFE & BRAIN GmbH and the University of Bonn.

AUTHOR CONTRIBUTIONS

Jannis Wißfeld: Conceptualization, data curation, formal analysis, investigation, methodology, and writing—original draft. **Ichiro Nozaki**: Conceptualization, data curation, formal analysis, investigation, methodology, and writing— original draft. **Mona Mathews**: Conceptualization, investigation and methodology, writing—review and editing. **Tamara Raschka**: Formal analysis, and writing—review and editing. **Christian Ebeling**: Formal analysis, and writing—review and editing. **Veit Hornung**: Funding acquisition, methodology, and writing—review and editing. **Oliver Brüstle**: Funding acquisition, methodology, and writing—review and editing. **Harald Neumann**: Conceptualization, funding acquisition, and writing—original draft and project administration.

DATA AVAILABILITY STATEMENT

The RNA-Seq data discussed in this publication have been deposited in NCBI's Gene Expression Omnibus (GEO) and are accessible through GEO Series accession number GSE155567 (https://www.ncbi.nlm.nih.gov/geo/query/acc.cgi?acc=GSE155567). Raw data and datasets are available from the corresponding author on reasonable request.

ETHICS APPROVAL

Ethics approval and consent to participate for generating the iPSC lines and their use for academic research were obtained by EBiSC.

ORCID

Harald Neumann https://orcid.org/0000-0002-5071-5202

REFERENCES

Alphey, M. S., Attrill, H., Crocker, P. R., & van Aalten, D. M. (2003). High resolution crystal structures of Siglec-7. Insights into ligand specificity in the Siglec family. *The Journal of Biological Chemistry*, *278*(5), 3372–3377. https://doi.org/10.1074/jbc.M210602200

Avril, T., Floyd, H., Lopez, F., Vivier, E., & Crocker, P. R. (2004). The membrane-proximal immunoreceptor tyrosine-based inhibitory motif is critical for the inhibitory signaling mediated by Siglecs-7 and -9, CD33-related Siglecs expressed on human monocytes and NK cells. *Journal of Immunology*, *173*(11), 6841–6849. https://doi.org/10.4049/jimmunol.173.11.6841

Bao, J., Wang, X. J., & Mao, Z. F. (2016). Associations between genetic variants in 19p13 and 19q13 regions and susceptibility to Alzheimer disease: A meta-analysis. *Medical Science Monitor*, *22*, 234–243.

Bhattacherjee, A., Rodrigues, E., Jung, J., Luzentales-Simpson, M., Enterina, J. R., Galleguillos, D., ... Macauley, M. S. (2019). Repression of phagocytosis by human CD33 is not conserved with mouse CD33. *Communications Biology*, *2*, 450. https://doi.org/10.1038/s42003-019-0698-6

Bourgin-Hierle, C., Gobert-Gosse, S., Therier, J., Grasset, M. F., & Mouchiroud, G. (2008). Src-family kinases play an essential role in differentiation signaling downstream of macrophage colony-stimulating factor receptors mediating persistent phosphorylation of phospholipase C-gamma2 and MAP kinases ERK1 and ERK2. *Leukemia*, *22*(1), 161–169. https://doi.org/10.1038/sj.leu.2404986

Bradshaw, E. M., Chibnik, L. B., Keenan, B. T., Ottoboni, L., Raj, T., Tang, A., ... de Jager, P. L. (2013). CD33 Alzheimer's disease locus: Altered monocyte function and amyloid biology. *Nature Neuroscience*, *16*(7), 848–850. https://doi.org/10.1038/nn.3435

Brinkman-Van der Linden, E. C., Angata, T., Reynolds, S. A., Powell, L. D., Hedrick, S. M., & Varki, A. (2003). CD33/Siglec-3 binding specificity, expression pattern, and consequences of gene deletion in mice. *Molecular and Cellular Biology*, *23*(12), 4199–4206. https://doi.org/10.1128/mcb.23.12.4199-4206.2003

Brosig, A., Kuhrt, H., Wiedemann, P., Kohen, L., Bringmann, A., & Hollborn, M. (2015). Gene expression regulation in retinal pigment epithelial cells induced by viral RNA and viral/bacterial DNA. *Molecular Vision*, *21*, 1000–1016.

Callaway, J. B., Smith, S. A., McKinnon, K. P., de Silva, A. M., Crowe, J. E., & Ting, J. P. (2015). Spleen tyrosine kinase (Syk) mediates IL-1β induction by primary human monocytes during antibody-enhanced dengue virus infection. *The Journal of Biological Chemistry*, *290*(28), 17306–17320. https://doi.org/10.1074/jbc.M115.664136

Carlson, M. (2019). org.Hs.eg.db: Genome wide annotation for Human.

Claude, J., Linnartz-Gerlach, B., Kudin, A. P., Kunz, W. S., & Neumann, H. (2013). Microglial CD33-related Siglec-E inhibits neurotoxicity by preventing the phagocytosis-associated oxidative burst. *The Journal of Neuroscience*, *33*(46), 18270–18276. https://doi.org/10.1523/jneurosci.2211-13.2013

Crocker, P. R., & Redelinghuys, P. (2008). Siglecs as positive and negative regulators of the immune system. *Biochemical Society Transactions*, *36*(Pt 6), 1467–1471. https://doi.org/10.1042/BST0361467

Crowley, M. T., Costello, P. S., Fitzer-Attas, C. J., Turner, M., Meng, F., Lowell, C., ... DeFranco, A. L. (1997). A critical role for Syk in signal transduction and phagocytosis mediated by Fcgamma receptors on macrophages. *The Journal of Experimental Medicine*, *186*(7), 1027–1039. https://doi.org/10.1084/jem.186.7.1027

Dobin, A., Davis, C. A., Schlesinger, F., Drenkow, J., Zaleski, C., Jha, S., ... Gingeras, T. R. (2013). STAR: ultrafast universal RNA-seq aligner. *Bioinformatics*, *29*(1), 15–21. https://doi.org/10.1093/bioinformatics/bts635

Freeman, S. D., Kelm, S., Barber, E. K., & Crocker, P. R. (1995). Characterization of CD33 as a new member of the sialoadhesin family of cellular interaction molecules. *Blood*, *85*(8), 2005–2012.

Gaikwad, S., Larionov, S., Wang, Y., Dannenberg, H., Matozaki, T., Monsonego, A., ... Neumann, H. (2009). Signal regulatory protein-beta1: A microglial modulator of phagocytosis in Alzheimer's disease. *The American Journal of Pathology*, *175*(6), 2528–2539. https://doi.org/10.2353/ajpath.2009.090147

Graham, D. B., Stephenson, L. M., Lam, S. K., Brim, K., Lee, H. M., Bautista, J., ... Swat, W. (2007). An ITAM-signaling pathway controls cross-presentation of particulate but not soluble antigens in dendritic cells. *The Journal of Experimental Medicine*, *204*(12), 2889–2897. https://doi.org/10.1084/jem.20071283

Griciuc, A., Serrano-Pozo, A., Parrado, A. R., Lesinski, A. N., Asselin, C. N., Mullin, K., ... Tanzi, R. E. (2013). Alzheimer's disease risk gene CD33

inhibits microglial uptake of amyloid beta. *Neuron*, 78(4), 631–643. https://doi.org/10.1016/j.neuron.2013.04.014

Gruber, R. C., LaRocca, D., Minchenberg, S. B., Christophi, G. P., Hudson, C. A., Ray, A. K., ... Massa, P. T. (2015). The control of reactive oxygen species production by SHP-1 in oligodendrocytes. *Glia*, 63(10), 1753–1771. https://doi.org/10.1002/glia.22842

Hollingworth, P., Harold, D., Sims, R., Gerrish, A., Lambert, J. C., Carrasquillo, M. M., ... Williams, J. (2011). Common variants at ABCA7, MS4A6A/MS4A4E, EPHA1, CD33 and CD2AP are associated with Alzheimer's disease. *Nature Genetics*, 43(5), 429–435. https://doi.org/10.1038/ng.803

Kant, A. M., De, P., Peng, X., Yi, T., Rawlings, D. J., Kim, J. S., & Durden, D. L. (2002). SHP-1 regulates Fcgamma receptor-mediated phagocytosis and the activation of RAC. *Blood*, 100(5), 1852–1859.

Krakauer, M., Sorensen, P., Khademi, M., Olsson, T., & Sellebjerg, F. (2008). Increased IL-10 mRNA and IL-23 mRNA expression in multiple sclerosis: Interferon-beta treatment increases IL-10 mRNA expression while reducing IL-23 mRNA expression. *Multiple Sclerosis*, 14(5), 622–630. https://doi.org/10.1177/1352458507087136

Krotz, F., Engelbrecht, B., Buerkle, M. A., Bassermann, F., Bridell, H., Gloe, T., ... Sohn, H. Y. (2005). The tyrosine phosphatase, SHP-1, is a negative regulator of endothelial superoxide formation. *Journal of the American College of Cardiology*, 45(10), 1700–1706. https://doi.org/10.1016/j.jacc.2005.02.039

Lajaunias, F., Dayer, J. M., & Chizzolini, C. (2005). Constitutive repressor activity of CD33 on human monocytes requires sialic acid recognition and phosphoinositide 3-kinase-mediated intracellular signaling. *European Journal of Immunology*, 35(1), 243–251. https://doi.org/10.1002/eji.200425273

Lambert, J. C., Ibrahim-Verbaas, C. A., Harold, D., Naj, A. C., Sims, R., Bellenguez, C., ... Amouyel, P. (2013). Meta-analysis of 74,046 individuals identifies 11 new susceptibility loci for Alzheimer's disease. *Nature Genetics*, 45(12), 1452–1458. https://doi.org/10.1038/ng.2802

Lawrence, D. W., & Koenig, J. M. (2012). Enhanced phagocytosis in neonatal monocyte-derived macrophages is associated with impaired SHP-1 signaling. *Immunological Investigations*, 41(2), 129–143. https://doi.org/10.3109/08820139.2011.595471

Liao, Y., Smyth, G. K., & Shi, W. (2014). featureCounts: An efficient general purpose program for assigning sequence reads to genomic features. *Bioinformatics*, 30(7), 923–930. https://doi.org/10.1093/bioinformatics/btt656

Linnartz, B., Kopatz, J., Tenner, A. J., & Neumann, H. (2012). Sialic acid on the neuronal glycocalyx prevents complement C1 binding and complement receptor-3-mediated removal by microglia. *The Journal of Neuroscience*, 32(3), 946–952. https://doi.org/10.1523/jneurosci.3830-11.2012

Love, M. I., Huber, W., & Anders, S. (2014). Moderated estimation of fold change and dispersion for RNA-seq data with DESeq2. *Genome Biology*, 15(12), 550. https://doi.org/10.1186/s13059-014-0550-8

Lowell, C. A. (2011). Src-family and Syk kinases in activating and inhibitory pathways in innate immune cells: Signaling cross talk. *Cold Spring Harbor Perspectives in Biology*, 3(3), 1–16. https://doi.org/10.1101/cshperspect.a002352

Lyons, B. L., Lynes, M. A., Burzenski, L., Joliat, M. J., Hadjout, N., & Shultz, L. D. (2003). Mechanisms of anemia in SHP-1 protein tyrosine phosphatase-deficient "viable motheaten" mice. *Experimental Hematology*, 31(3), 234–243.

Maeda, A., Kurosaki, M., Ono, M., Takai, T., & Kurosaki, T. (1998). Requirement of SH2-containing protein tyrosine phosphatases SHP-1 and SHP-2 for paired immunoglobulin-like receptor B (PIR-B)-mediated inhibitory signal. *The Journal of Experimental Medicine*, 187(8), 1355–1360. https://doi.org/10.1084/jem.187.8.1355

Maeda, A., Scharenberg, A. M., Tsukada, S., Bolen, J. B., Kinet, J. P., & Kurosaki, T. (1999). Paired immunoglobulin-like receptor B (PIR-B) inhibits BCR-induced activation of Syk and Btk by SHP-1. *Oncogene*, 18(14), 2291–2297. https://doi.org/10.1038/sj.onc.1202552

Malik, M., Simpson, J. F., Parikh, I., Wilfred, B. R., Fardo, D. W., Nelson, P. T., & Estus, S. (2013). CD33 Alzheimer's risk-altering polymorphism, CD33 expression, and exon 2 splicing. *The Journal of Neuroscience*, 33(33), 13320–13325. https://doi.org/10.1523/JNEUROSCI.1224-13.2013

Matozaki, T., Murata, Y., Okazawa, H., & Ohnishi, H. (2009). Functions and molecular mechanisms of the CD47-SIRPalpha signalling pathway. *Trends in Cell Biology*, 19(2), 72–80. https://doi.org/10.1016/j.tcb.2008.12.001

May, A. P., Robinson, R. C., Vinson, M., Crocker, P. R., & Jones, E. Y. (1998). Crystal structure of the N-terminal domain of sialoadhesin in complex with 3′ sialyllactose at 1.85 A resolution. *Molecular Cell*, 1(5), 719–728.

Mocsai, A., Abram, C. L., Jakus, Z., Hu, Y., Lanier, L. L., & Lowell, C. A. (2006). Integrin signaling in neutrophils and macrophages uses adaptors containing immunoreceptor tyrosine-based activation motifs. *Nature Immunology*, 7(12), 1326–1333. https://doi.org/10.1038/ni1407

Naj, A. C., Jun, G., Beecham, G. W., Wang, L. S., Vardarajan, B. N., Buros, J., ... Schellenberg, G. D. (2011). Common variants at MS4A4/MS4A6E, CD2AP, CD33 and EPHA1 are associated with late-onset Alzheimer's disease. *Nature Genetics*, 43(5), 436–441. https://doi.org/10.1038/ng.801

Neznanov, N., Neznanova, L., Kondratov, R. V., Burdelya, L., Kandel, E. S., O'Rourke, D. M., ... Gudkov, A. V. (2003). Dominant negative form of signal-regulatory protein-alpha (SIRPalpha /SHPS-1) inhibits tumor necrosis factor-mediated apoptosis by activation of NF-kappa B. *The Journal of Biological Chemistry*, 278(6), 3809–3815. https://doi.org/10.1074/jbc.M210698200

Okenwa, C., Kumar, A., Rego, D., Konarski, Y., Nilchi, L., Wright, K., & Kozlowski, M. (2013). SHP-1-Pyk2-Src protein complex and p38 MAPK pathways independently regulate IL-10 production in lipopolysaccharide-stimulated macrophages. *Journal of Immunology*, 191(5), 2589–2603. https://doi.org/10.4049/jimmunol.1300466

Paul, S. P., Taylor, L. S., Stansbury, E. K., & McVicar, D. W. (2000). Myeloid specific human CD33 is an inhibitory receptor with differential ITIM function in recruiting the phosphatases SHP-1 and SHP-2. *Blood*, 96(2), 483–490.

RStudio Team. (2015). *RStudio: Integrated development for R*. Vienna, Austria: RStudio.

R Core Team. (2018). *R: A language and environment for statistical computing*. Vienna, Austria: R Core Team.

Raj, T., Ryan, K. J., Replogle, J. M., Chibnik, L. B., Rosenkrantz, L., Tang, A., ... Bradshaw, E. M. (2014). CD33: Increased inclusion of exon 2 implicates the Ig V-set domain in Alzheimer's disease susceptibility. *Human Molecular Genetics*, 23, 2729–2736.

Raju, T. S., Briggs, J. B., Borge, S. M., & Jones, A. J. S. (2000). Species-specific variation in glycosylation of IgG: evidence for the species-specific sialylation and branch-specific galactosylation and importance for engineering recombinant glycoprotein therapeutics. *Glycobiology*, 10(5), 477–486. http://dx.doi.org/10.1093/glycob/10.5.477

Rasmussen, M. A., Holst, B., Tümer, Z., Johnsen, M. G., Zhou, S., Stummann, T. C., ... Clausen, C. (2014). Transient p53 suppression increases reprogramming of human fibroblasts without affecting Apoptosis and DNA Damage. *Stem Cell Reports*, 3(3), 404–413. http://dx.doi.org/10.1016/j.stemcr.2014.07.006

Rego, D., Kumar, A., Nilchi, L., Wright, K., Huang, S., & Kozlowski, M. (2011). IL-6 production is positively regulated by two distinct Src homology domain 2-containing tyrosine phosphatase-1 (SHP-1)-dependent CCAAT/enhancer-binding protein beta and NF-kappaB pathways and an SHP-1-independent NF-kappaB pathway in lipopolysaccharide-stimulated bone marrow-derived macrophages. *Journal of Immunology*, 186(9), 5443–5456. https://doi.org/10.4049/jimmunol.1003551

Salminen, A., & Kaarniranta, K. (2009). Siglec receptors and hiding plaques in Alzheimer's disease. *Journal of Molecular Medicine (Berlin, Germany)*, 87(7), 697–701. https://doi.org/10.1007/s00109-009-0472-1

Schmid-Burgk, J. L., Schmidt, T., Gaidt, M. M., Pelka, K., Latz, E., Ebert, T. S., & Hornung, V. (2014). OutKnocker: A web tool for rapid and simple genotyping of designer nuclease edited cell lines. *Genome Research*, 24(10), 1719–1723. https://doi.org/10.1101/gr.176701.114

Schmidt, T., Schmid-Burgk, J. L., Ebert, T. S., Gaidt, M. M., & Hornung, V. (2016). Designer nuclease-mediated generation of knockout THP1 cells. *Methods in Molecular Biology*, 1338, 261–272. https://doi.org/10.1007/978-1-4939-2932-0_19

Schmidt, T., Schmid-Burgk, J. L., & Hornung, V. (2015). Synthesis of an arrayed sgRNA library targeting the human genome. *Scientific Reports*, 5, 14987. https://doi.org/10.1038/srep14987

Shahraz, A., Kopatz, J., Mathy, R., Kappler, J., Winter, D., Kapoor, S., … Neumann, H. (2015). Anti-inflammatory activity of low molecular weight polysialic acid on human macrophages. *Scientific Reports*, 5, 16800. https://doi.org/10.1038/srep16800

Siddiqui, S. S., Springer, S. A., Verhagen, A., Sundaramurthy, V., Alisson-Silva, F., Jiang, W., … Varki, A. (2017). The Alzheimer's disease-protective CD33 splice variant mediates adaptive loss of function via diversion to an intracellular pool. *The Journal of Biological Chemistry*, 292(37), 15312–15320. https://doi.org/10.1074/jbc.M117.799346

Slack, E. C., Robinson, M. J., Hernanz-Falcon, P., Brown, G. D., Williams, D. L., Schweighoffer, E., … Reise Sousa, C. (2007). Syk-dependent ERK activation regulates IL-2 and IL-10 production by DC stimulated with zymosan. *European Journal of Immunology*, 37(6), 1600–1612. https://doi.org/10.1002/eji.200636830

Szumanska, G., Vorbrodt, A. W., Mandybur, T. I., & Wisniewski, H. M. (1987). Lectin histochemistry of plaques and tangles in Alzheimer's disease. *Acta Neuropathologica*, 73(1), 1–11.

Takahashi, K., Rochford, C. D., & Neumann, H. (2005). Clearance of apoptotic neurons without inflammation by microglial triggering receptor expressed on myeloid cells-2. *The Journal of Experimental Medicine*, 201(4), 647–657. https://doi.org/10.1084/jem.20041611

Taylor, V. C., Buckley, C. D., Douglas, M., Cody, A. J., Simmons, D. L., & Freeman, S. D. (1999). The myeloid-specific sialic acid-binding receptor, CD33, associates with the protein-tyrosine phosphatases, SHP-1 and SHP-2. *The Journal of Biological Chemistry*, 274(17), 11505–11512.

Varki, A. (2001). Loss of N-glycolylneuraminic acid in humans: Mechanisms, consequences, and implications for hominid evolution. *American Journal of Physical Anthropology*, 116(S33), 54–69. http://dx.doi.org/10.1002/ajpa.10018

Walter, R. B., Appelbaum, F. R., Estey, E. H., & Bernstein, I. D. (2012). Acute myeloid leukemia stem cells and CD33-targeted immunotherapy. *Blood*, 119, 6198–6208.

Walter, R. B., Raden, B. W., Zeng, R., Hausermann, P., Bernstein, I. D., & Cooper, J. A. (2008). ITIM-dependent endocytosis of CD33-related Siglecs: Role of intracellular domain, tyrosine phosphorylation, and the tyrosine phosphatases, Shp1 and Shp2. *Journal of Leukocyte Biology*, 83(1), 200–211. https://doi.org/10.1189/jlb.0607388

Wang, Y., & Neumann, H. (2010). Alleviation of neurotoxicity by microglial human Siglec-11. *The Journal of Neuroscience*, 30(9), 3482–3488. https://doi.org/10.1523/jneurosci.3940-09.2010

Wickham, H. (2016). *ggplot2: Elegant graphics for data analysis*. New York, NY: Springer-Verlag.

Yu, G., Wang, L. G., Han, Y., & He, Q. Y. (2012). clusterProfiler: An R package for comparing biological themes among gene clusters. *Omics*, 16(5), 284–287. https://doi.org/10.1089/omi.2011.0118

Zaric, S. S., Lappin, M. J., Fulton, C. R., Lundy, F. T., Coulter, W. A., & Irwin, C. R. (2017). Sialylation of Porphyromonas gingivalis LPS and its effect on bacterial-host interactions. *Innate Immunity*, 23(3), 319–326. https://doi.org/10.1177/1753425917694245

Zhang, B., Gaiteri, C., Bodea, L. G., Wang, Z., McElwee, J., Podtelezhnikov, A. A., … Emilsson, V. (2013). Integrated systems approach identifies genetic nodes and networks in late-onset Alzheimer's disease. *Cell*, 153(3), 707–720. https://doi.org/10.1016/j.cell.2013.03.030

Zhu, A., Ibrahim, J. G., & Love, M. I. (2019). Heavy-tailed prior distributions for sequence count data: Removing the noise and preserving large differences. *Bioinformatics*, 35(12), 2084–2092. https://doi.org/10.1093/bioinformatics/bty895

Ziegenfuss, J. S., Biswas, R., Avery, M. A., Hong, K., Sheehan, A. E., Yeung, Y. G., … Freeman, M. R. (2008). Draper-dependent glial phagocytic activity is mediated by Src and Syk family kinase signalling. *Nature*, 453(7197), 935–939. https://doi.org/10.1038/nature06901

SUPPORTING INFORMATION

Additional supporting information may be found online in the Supporting Information section at the end of this article.